Petroleum Science 22 (2025) 110–129

Contents lists available at ScienceDirect

Petroleum Science

journal homepage: www.keaipublishing.com/en/journals/petroleum-science

Original Paper

Sub-lacustrine debrite system: Facies architecture and sediment distribution pattern

Jian-Ping Liu [a, b], Ben-Zhong Xian [c, d, *], Xian-Feng Tan [a, b, **], Zhen Wang [e], Jun-Hui Wang [c, d], Long Luo [a, b], Peng Chen [f], Yan-Xin He [g], Rong-Heng Tian [c, d], Qian-Ran Wu [c, d], Jia Wang [a, b], Jin Li [h], Long Chen [a], Wen-Yi Peng [a], Yi-Man Zhou [a], Quan-Feng Jiang [a]

[a] School of Petroleum Engineering, Chongqing University of Science and Technology, Chongqing, 401331, China
[b] Chongqing Key Laboratory of Complex Oil and Gas Field Exploration and Development, Chongqing University of Science and Technology, Chongqing, 401331, China
[c] National Key Laboratory of Petroleum Resources and Engineering, China University of Petroleum (Beijing), Beijing, 102249, China
[d] College of Geosciences, China University of Petroleum (Beijing), Beijing 102249, China
[e] Jidong Oilfield of CNPC, Tangshan, Hebei, 063000, China
[f] School of Earth Sciences and Resources, China University of Geosciences (Beijing), Beijing, 100083, China
[g] School of Earth and Space Sciences, Peking University, Beijing, 100871, China
[h] Petroleum Exploration & Production Research Institute, SINOPEC, Beijing, 102206, China

ARTICLE INFO

Article history:
Received 20 July 2022
Received in revised form
28 June 2024
Accepted 11 November 2024
Available online 18 November 2024

Edited by Teng Zhu

Keywords:
Deep-water deposition
Sediment gravity flow
Debris flow
Lacustrine basin
Bohai Bay basin

ABSTRACT

The deep-water systems in different types of sedimentary basins exhibit significant variability. Current knowledge of deep-water deposition is mainly derived from deep-marine turbidite systems. However, the characteristics and differences of sub-lacustrine gravity flow deposition systems have been a research focus in the fields of sedimentology and petroleum geology. This study investigates the facies architecture, depositional processes, and sediment distribution patterns of a sub-lacustrine debrite system in the Eocene Dongying Rift of the Bohai Bay Basin, China, through the analysis of integrated core data, 3-D seismic data, and well-log data. Nine facies have been identified within the debrite system, representing various depositional processes such as sandy debris flow, muddy debris flow, turbidity currents, sandy slide, sandy slide/slump, and mud flow. Our research indicates that the sub-lacustrine system is primarily influenced by debris flow rather than turbidity currents, as supported by facies quantification, interpretation, and flow rheology analysis. Additionally, we have identified five basic facies building blocks in debrite systems, including slide masses, slump masses, debrite channels, debrite lobes, and turbidite sheets. We have also elucidated and proposed detailed sedimentary processes, flow transport, and transformation within the sub-lacustrine system through analysis of flow origins, facies sequences, and distribution characteristics. Our findings highlight the evolutionary progression from delta-front collapse to sandy slide/slump, sandy debris flow, and finally muddy debris flow. The efficient generation of turbidity currents from parental landslides on sand-prone slopes is deemed unlikely due to rift-basin morphology and transport distances. The formation of the five basic facies building blocks is closely linked to depositional processes and dominant flow types. Consequently, we present a deep-water depositional model for sub-lacustrine debrite systems, focusing on flow dynamics, sediment distribution patterns, and basin morphology within deep lacustrine rifts. This model offers valuable insights into the variability of deep-water deposition in diverse basin settings and aids in predicting lithologic reservoirs during deep-water hydrocarbon exploration.

1. Introduction

Gravity flows are the most important transportation process for terrigenous clastic delivery to deep-basin, giving rise to huge

* Corresponding author. National Key Laboratory of Petroleum Resources and Engineering, China.
** Corresponding author. Chongqing University of Science and Technology, China.
E-mail addresses: xianbzh@cup.edu.cn (B.-Z. Xian), xianfengtan8299@163.com (X.-F. Tan).

https://doi.org/10.1016/j.petsci.2024.11.007
1995-8226/

sediment accumulations (Talling et al., 2007; Mutti et al., 2009; Zavala and Arcuri, 2016; Shanmugam, 2016; Bailey et al., 2021; Liu et al., 2021, 2022; Liu et al., 2022; Chen et al., 2023) and significant hydrocarbon reserves (Stow and Johansson, 2000; Weimer and Pettingill, 2007; Xian et al., 2018; Yang et al., 2023). In recent decades, the study of deep-water gravity flows and their associated deposits has gained increasing attention due to their importance in sequence stratigraphy, climate reconstruction, source-to-sink sedimentology, hazard assessment, and hydrocarbon exploration (Piper and Aksu, 1987; Stow and Mayall, 2000; Steel al., 2002; Sømme et al., 2009; Kremer et al., 2015; Gong et al., 2016; Yang et al., 2017; Wang et al., 2020; Chen et al., 2021).

Debris flows represent the key member as well as turbidity currents in the gravity flow family (Hampton, 1972; Middleton and Hampton, 1973, 1976; Stow and Mayall, 2000; Talling et al., 2012; Talling, 2014; Dodd et al., 2022), which has been typically distinguished and documented in modern and ancient deep-water environments as well as on land (Cronin et al., 1998; Talling et al., 2007; Migeon et al., 2010; Ducassou et al., 2016; Peng, 2021; Cao et al., 2021; Tan et al., 2022; Peng et al., 2022). The deposits of debris flow usually contribute significant petroleum reservoirs and thus has received much attention in recent years (Shanmugam et al., 1994; Stow and Johansson, 2000; Zou et al., 2012; Shanmugam, 2013; Xian et al., 2014, 2017, 2018; Li et al., 2016; Liu et al., 2017; Liu et al., 2022). Previous studies indicate that debris flow deposits may significantly developed in some deep-water settings (Laberg and Vorren, 1995; Elverhøi et al., 1997; Gardner et al., 2000; Talling et al., 2007; Zou et al., 2012; Liu et al., 2017), and they may occur as a major component in an idealized slump-initiated process (Shanmugam, 2000).

In deep-water environments, debris flows typically exhibit 'en masse' deposition (Johnson, 1970; Coussot and Meunier, 1996; Zou et al., 2012; Wu et al., 2022). The external morphology of single-phase debris flow deposits commonly appears as tongue-shaped bodies (Laberg and Vorren, 1995; Elverhøi et al., 1997; Shanmugam, 2016). The external morphology of single-phase debris flow deposits commonly appears as tongue-shaped bodies (Liu et al., 2017), and in debris flow dominated systems, the development of MTDs is typically associated (Shanmugam, 2000). However, in traditional turbidite systems, sedimentation is primarily controlled by turbidity currents (Mutti et al., 2009). The Bouma Sequence and submarine fan are key concepts in traditional turbidite systems (Bouma, 1962; Normark, 1970; Walker, 1978). A submarine fan typically comprises three parts: inner fan, middle-fan, and outer fan. The inner fan mainly consists of a feeder channel; the middle-fan contains multiple distributary channels and lobe complexes, with the lobe complex further divided into lobe, lobe element, and bed as multiple hierarchical depositional elements (Prélat et al., 2009, 2010). The outer fan is mainly composed of thin-bedded sheet-like turbidites and deep-sea mud. Overall, the different parts of a submarine fan can be described by the different divisions of the turbidite Bouma Sequence (Bouma, 1962; Normark, 1970; Walker, 1978). Currently, compared to traditional turbidite systems, there is a lack of understanding regarding the facies architecture and dispersal pattern of deep-water debris flow dominated systems (Normark, 1970; Walker, 1978; Reading and Richards, 1994; Posamentier and Kolla, 2003). Therefore, further investigations are needed to quantify and evaluate the contributions and importance of debris flow in deep basin stratigraphic record.

Moreover, deep-water gravity flow transport and transformation have been long concerned and is still the subject on debate due to its importance in understanding deep-water depositional process and sediment accumulation. Recently, increasing studies have been focused on the flow process in turbidite systems, which reveal that high-density turbidity current can gradually transform into distal cohesive clay-rich debris flow and low-density turbidity current (Haughton et al., 2003; Kane and Pontén, 2012; Southern et al., 2017; Yang et al., 2020; Peng, 2021; Tan et al., 2022), whereas the discussions on flow transformation in subaqueous debris flow dominated process are really rare (Shanmugam et al., 1994; Zou et al., 2012), and it remains uncertainty whether the observed transformation between turbidity current and debris flow in flumes or outcrops (Mohrig et al., 1998; Sohn, 2000; Felix and Peakall, 2006; Ito, 2008; Felix et al., 2009; Southern et al., 2017) can be immediately extrapolated to understand the whole picture of sediments transport in deep-water debrite systems.

The Middle Sub-member of the third Member of the Eocene Shahejie Formation in the Dongying lacustrine rift provides well-developed sand-rich deep-water facies that have been analyzed by an integration of core data, seismic and well-log data to better understand the flow process and architectural model of deep-water depositional system in lacustrine rift basins. This study aims to: (1) identify and quantify different types of facies and facies associations of a sub-lacustrine debrite system; (2) reveal the origin of different facies and the whole picture of deep-water process of slump-derived gravity flows in a lacustrine rift basin; (3) recognition, location and characterization of deep-water architectural elements in sub-lacustrine slope to basin-floor settings; (4) establish a sediment dispersal model of broad significance for debrite system in deep rift-basins by taking into flow process, depositional architecture and controlling factors.

2. Geological background

The Dongying Rift, is a Mesozoic-Cenozoic asymmetrical half graben, which located in the southeast Bohai Bay Basin of the East China. The rift developed along a NW-SE trending and covers an area of nearly 5700 km^2. It is bounded by the Chenjiazhuang Rise in the north, the Luxi Uplift and Guangrao Rise in the south, the Qingcheng Rise in the west and the Qingtuozi Rise in the east (Fig. 1) (Cao et al., 2018).

Tectonically, the evolution of the Dongying Rift comprises two development stages, i.e. the syn-rift period in the Paleogene (~65.0–24.6 Ma), and the post-rift period in the Neogene (~24.6 Ma to the present) (Feng et al., 2016). The Paleogene syn-rift lacustrine sequence can be subdivided into Kongdian, Shahejie, and Dongying Formation from the bottom up. The Eocene Shahejie Formation consists of four members, Member 4 (Es4), Member 3 (Es3), Member 2 (Es2) and Member 1 (Es1) from oldest to newest (Hu et al., 2001; Liu et al., 2022). Member Es3 developed during the intense rifting episode, which commenced with the maximum lake depth of approximately 120–170 m (Li et al., 2005), can be further divided from bottom up as $Es3^l$ (the lower part), $Es3^m$ (the middle part) and $Es3^u$ (the upper part). Typically, the Es3 is characterized by dark-colored muds with interbedded sands (Fig. 2) (Jin et al., 2005).

During the formation of Member Es3 in the study area, the Dongying Delta constitutes the largest delta system and significantly shaped coeval paleogeomorphology and depositional setting (Fig. 1c). The delta started to form in the early Es3 and abandoned in the late Eocene, prograded along the SEE direction with its main development taking place in the $Es3^m$ (Feng et al., 2013). Because of the large amount of sediment supply, Dongying Delta forms large-scale prograded clinothems of hundreds of meters thick and promotes the development of large volumes accumulation of gravity flow deposits which provide significant oil and gas reservoirs. During the whole development period of the delta, fluvial-deltaic system can cover as much as 4300 km^2, which account for approximately 80% of the area of the Dongying Rift. The studied section is the $Es3^m$ which represent the main part of the delta-

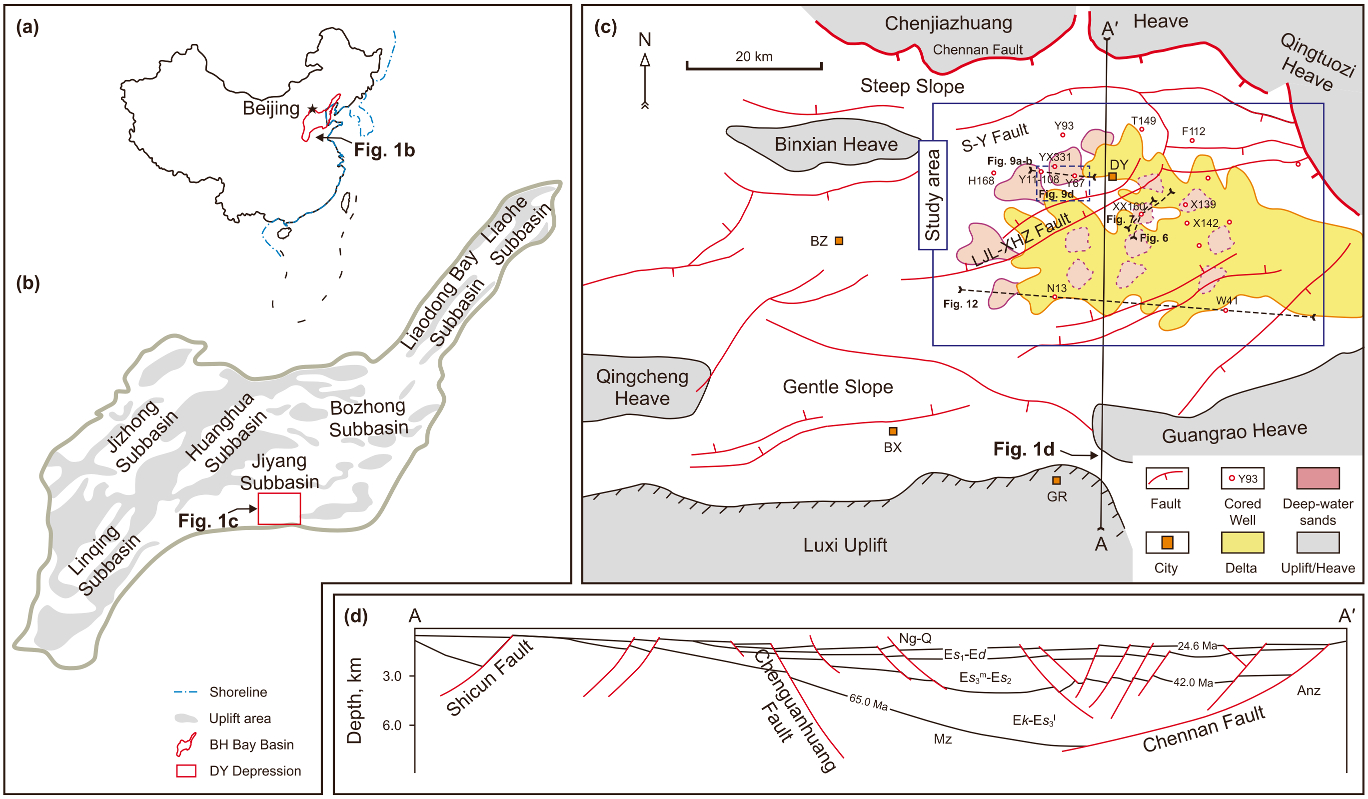

Fig. 1. (**a**) Regional map indicating the location of the Bohai Bay Basin. (**b**) Tectonic location of the Dongying Rift in the SE Bohai Bay Basin. (**c**) Map showing the study area in the Dongying Rift and the Eocene delta and turbidite system distribution. (**d**) Structure and strata interpretation across the Dongying Rift. See Fig. 1(**c**) for profile location. (after Feng et al., 2013).

debrite sequence, is consists of six parasequence sets (from PSS 6 to PSS 1 bottom-up) and developed mainly during lake level highstands (Fig. 2) (Qiu et al., 2001).

3. Data and method

The present study is based on the analysis of geological data from 60 exploration boreholes (cores, wireline logs) and 3-D seismic data covering approximately 1200 km^2 acquired from the Dongying Rift, Bohai Bay Basin by China National Petroleum Corporation. An integrated approach was used to examine the Eocene deep-lacustrine deposits in this area, combining information from cores, 3-D seismic and well-log data.

The seismic data were processed to zero phase, and the vertical resolution of seismic data varies with depth, while the dominant seismic frequency is approximately 35–40 Hz for the Member Es3^m of interest. The seismic sections were converted from time to depth using an average velocity value of 3600 m/s suggested by Feng et al. (2013) for the studied interval, which yields a vertical resolution (λ/4) of ca. 15–25 m. The characteristics and origin of resedimented deep-water facies were acquired from examination, identification and interpretation of approximately 968 m of conventional cores. Wireline log motifs were also applied to the deep-water depositional element recognition and interpretation according to the shapes and trends of SP (spontaneous potential) and GR (gamma-ray) logging curves. Additionally, exploration borehole data were tied to seismic profiles for calibration of seismic interpretations. Moreover, the RMS (root-mean-square) seismic amplitude map acquired from 3-D seismic survey by seismic imaging was used for better understanding of the distribution and arrangement of deep-water deposits.

4. Results

4.1. Facies and interpretation

A facies scheme was developed for the deep-water deposits in the Eocene Dongying Rift based on the examination of approximately 968 m cores (Table 1). Nine different resedimented facies types have been identified and classified to determine the flow mechanisms based on sediment grain-size, sedimentary structure and textural analysis.

4.1.1. Clean massive sandstone (Scm)

Description: Facies Scm is characterized by light gray colored, structureless, fine to medium grained, well to moderately sorted, grain-supported sandstones with very low content of mud matrix (<5%). Neither grading nor traction structures were observed (Fig. 3(a); Table 1). Facies Scm is generally closely interbedded with facies Sfc (i.e. massive sandstone with floating clasts), which are both encased within dark-colored mudstones and jointly contribute the most widespread resedimented facies in the study area.

Interpretation: Structureless texture without apparent vertical rhythm can indicate ‘en masse’ settling of sediments in debris flow (Johnson, 1970; Lowe, 1976, 1982; Shanmugam, 1996; Coussot and Meunier, 1996) and can be comparable with Ta division of Bouma sequence as well (Bouma, 1962), during which sediments rest rapidly due to the loss of the grain support mechanism (Middleton and Hampton, 1976; Lowe, 1976, 1982), and resultantly the differentiation of sediments is unlikely to happen. Additionally, clean massive sands have been also proved common in both ancient and modern deep-marine basins, which are generally interpreted as sandy debris flow deposition (i.e. cohesionless debris flow; Falk and

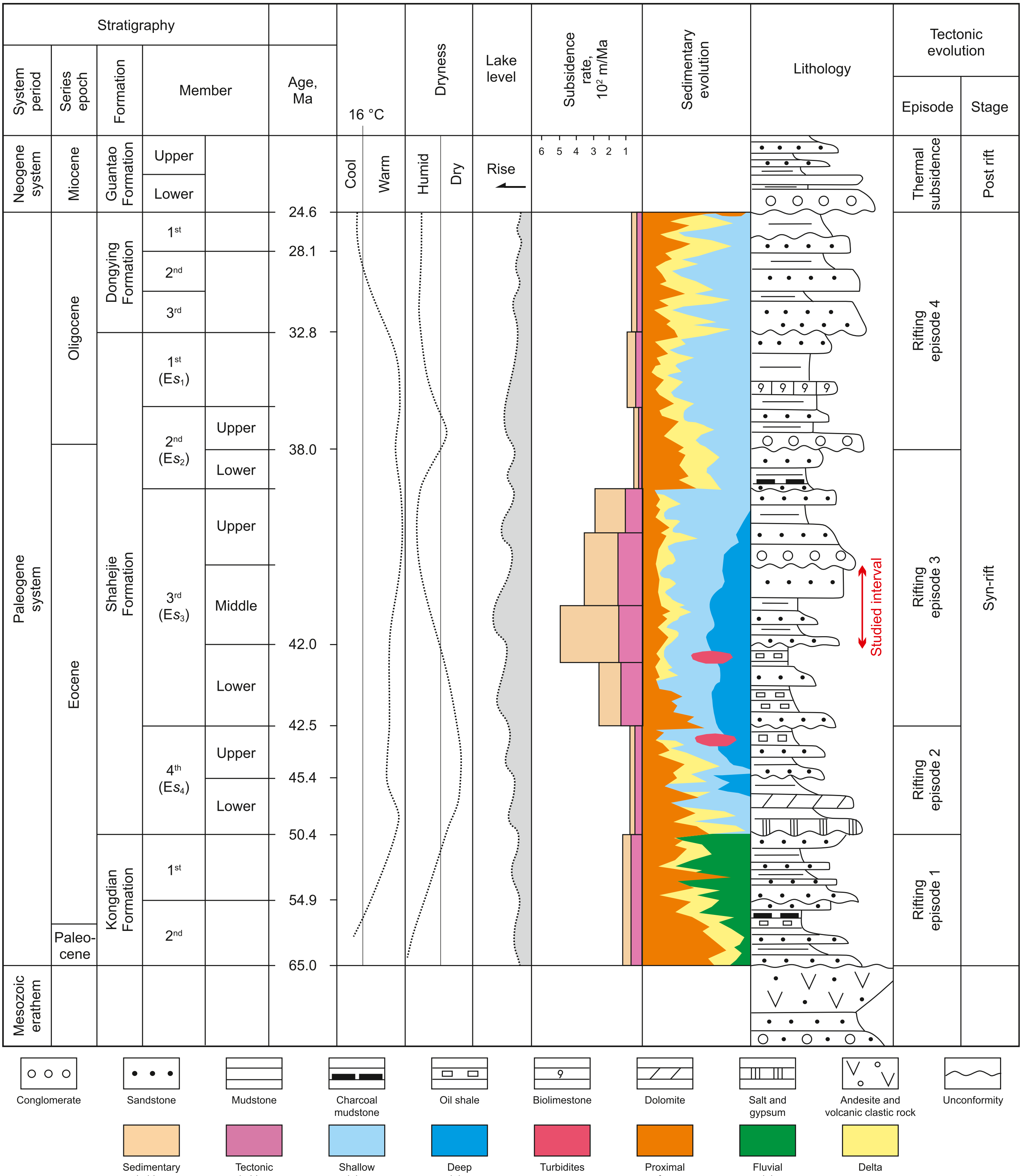

Fig. 2. Lithostratigraphic column of the Paleogene Dongying Rift (after Feng et al., 2016).

Dorsey, 1998; Stow and Johansson, 2000; Yang et al., 2020; Tian et al., 2023).

4.1.2. *Massive sandstone with floating clasts (Sfc)*

Description: Facies Sfc is characterized by light or dark gray colored, fine to medium grained, massive sands with floating sand or mud clasts (Fig. 3(b); Table 1). The matrix sands are generally moderately sorted, and the sand or mud clasts usually vary largely in size (from <1 cm to >10 cm), shape, position and orientation in sand beds. Generally, sand clasts usually display subrounded in

Table 1
Facies classification scheme for resedimented deposits in the Eocene Dongying Rift.

Lithofacies	Code	Features	Process	Interpretation
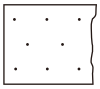 Clean massive sandstone	Scm	Ungraded sandstone clean and massive low in clay content	Debris flow Freezing Plastic rheology	Sandy debrites
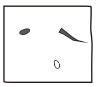 Massive sandstone with floating clasts	Sfc	Ungraded sand matrix rip-up mudclasts sand and mud pebbles planar to random clast fabrics	Debris flow Freezing Plastic rheology	Sandy debrites
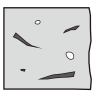 Massive muddy sandstone with floating clasts	MSfc	Massive and muddy mud rip-ups or floating gravel particles with random fabrics	Debris flow Freezing Plastic rheology	Muddy debrites
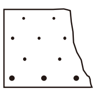 Normally graded sandstone	Sng	Normally grading slightly erosive base or non-erosive base	Turbidity current Suspended load Newtonian rheology	Turbidites Bouma Ta
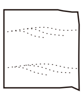 Wavy bedded sandstone	Swb	Fine-silt grained with wave ripples	Turbidity current Suspended load Newtonian rheology	Turbidites Bouma Tc
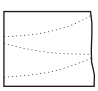 Cross bedded sandstone	Scb	Cross stratification fine grained	Slide Massive transport Elastic block	Sandy slides
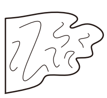 Deformed bedded (muddy) sandstone	Sdb	Contorted layers slump-folded heterolithic facies	Slump Massive transport Elastic-plastic block	Sandy slumps
 Deformed bedded (sandy) mudstone	Mdb	Contorted layers slump-folded heterolithic facies	Slump Massive transport Elastic-plastic block	Muddy slumps
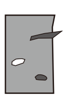 Massive mudstone with floating clasts	Mfc	Massive structure sand or mud clasts usually random fabrics	Debris flowFreezing Plastic rheology	Mudflow deposits

shape while mud clasts can be subrounded or rip-ups. Sand or mud clasts can take place at the base, or in the middle, or display as rafted clasts at the top of the sand bed, and generally distribute parallel to the bedding plane, displaying planar fabrics, or exhibit random fabrics (Fig. 3(b)). Additionally, terrestrial plant debris can be occasionally observed in these facies.

Interpretation: The ungraded sands and nearly vertically distributed clasts (random fabric) (Fig. 3(b)) in sand matrix represent the final position while the sediments freezing en masse in plastic flows (Enos, 1977; Amy et al., 2005; Peng, 2021; Peng et al., 2022; Wu et al., 2022). Planar clast fabric is the indication of fully laminar shear straining flow during transportation (Fisher, 1971; Hampton, 1975; Dasgupta, 2003). Rafted clasts closely located to the upper surface of massive sandstone beds which exhibit an inverse grading (Fig. 3(b)) is similar to the documented deep-sea sandy debrite and flume observations (Postma et al., 1988; Soh, 1989; Shanmugam, 1996; Kim et al., 1995), which can be attributed to the results of low shear at debris flow front (Parsons et al., 2001) or smaller grains percolating downward through big voids due to kinetic sieving, or buoyant lift (Iverson, 1997). Accordingly, this typical and ubiquitous facies (Sfc) in the studied interval, is attributed to sandy debrite.

4.1.3. *Massive muddy sandstone with floating clasts (MSfc)*

Description: Facies MSfc comprises gray or dark gray colored, massive and muddy sands with floating rip-ups (Fig. 3(c); Table 1). Facies MSfc generally interbedded with massive sands. MSfc units can vary greatly in thickness from very thin (in centimeter scale) to very thick (>5 m). Floating rip-ups in these facies are mostly less than 10 cm in length, angular to subrounded in shape, and generally show planar fabrics (Fig. 3(c)).

Interpretation: Both muddy and sandy debris flow is characterized by a finite yield strength, which can be resulted from cohesive strength as well as frictional strength of the material (Dasgupta, 2003). As a result, freeze ‘en masse’ would occur in muddy debris flow due to cohesive grain resistance (i.e. cohesive freezing), or frictional grain resistance (i.e. frictional freezing) while the shear force exerted by the downslope component of gravitational pull falls below the yield strength (Johnson, 1970; Coussot and Meunier, 1996). Many features in MSfc can suggest muddy debris flow origin. Floating clasts with random fabrics indicate plug-flow conditions and freezing deposition by debris flows en masse. Planar fabrics of floating clasts reveal laminar flow and plastic rheology, which indicate interfacial shear between the floating clasts and cohesive, mud-rich matrix.

4.1.4. *Normally graded sandstone (Sng)*

Description: Facies Sng consists of light gray or gray colored, fine to very fine grained sands with normal grading, this facies units exbihit thin bedded layers in centimeter scale and generally less than 0.2 m in thick (Fig. 3(d); Table 1). These facies commonly interbedded with upper laminated dark-colored muds, showing

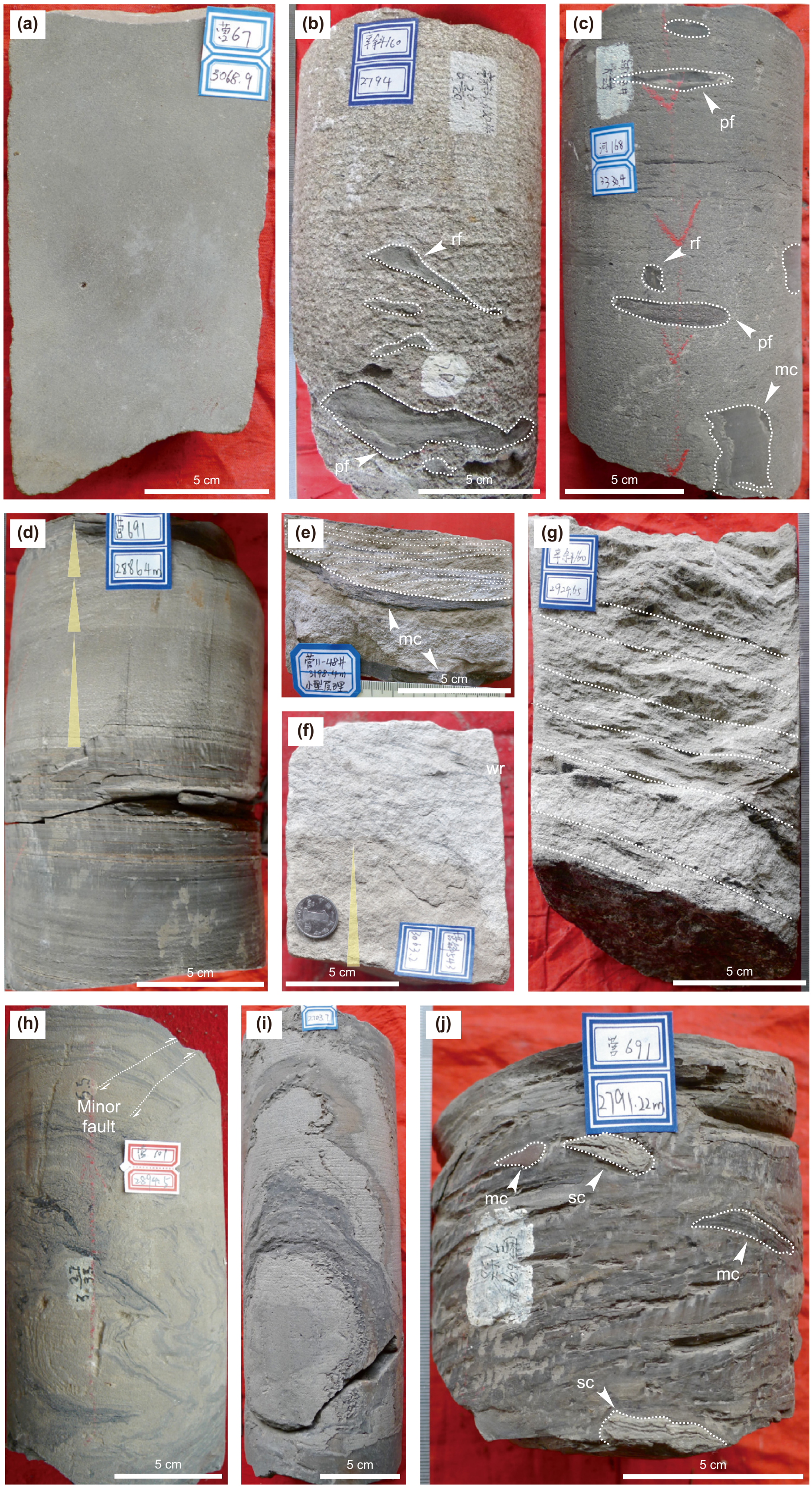

Fig. 3. Representative core photographs of resedimented facies in the Eocene Dongying Rift. Clean massive sandstone without apparent sedimentary structures (**a**); massive sandstones with floating clasts and amalgamation surface showing sharp and parallel contact, clasts are generally subrounded or mud rip-ups (**b**); massive muddy sandstone with floating clasts (**c**); normally graded sandstone with underlying dark-colored laminated mudstone (**d**); wavy bedded sandstone with underlying massive sandstone (**e**) and wavy

rhythmic bedding, and the base of these units may display planar or slightly erosive contact with lower muds.

Interpretation: The fining-up grain size trends in facies Sng can be attributed to the deposition by suspension and settling in turbidity currents. The normally graded sands indicate the classic Bouma Ta division (Bouma, 1962), and generally represent velocity decreases in surge-like waning turbulent flows (Sanders, 1965; Mulder and Alexander, 2001). Erosional base of facies Sng can suggest the erosive power of turbulent gravity flows.

4.1.5. Wavy bedded sandstone (Swb)

Description: Facies Swb comprises light gray to gray colored, very-fine to silty sands with wave ripples (Fig. 3(e) and (f); Table 1). Beds consists of facies Swb are generally less than 0.2 m in thick, they commonly distributed locally and occur with lower massive or normally graded sand units and upper laminated muds.

Interpretation: The wavy bedded intervals occurred in deep-water settings can be interpretated as traction by low-density turbidity flows, which can be comparable with the Bouma Tc unit (Bouma, 1962). Recently, they were also frequently observed in hybrid event beds with linked debrites (i.e. H3 division of HEB) which can be attributed to the flow energy decreases (Haughton et al., 2009).

4.1.6. Cross bedded sandstone (Scb)

Description: Facies Scb is characterized by light gray, fine or medium grained sands with trough or tabular cross-bedding. Very thin mud layers which are usually discontinuous can be commonly observed paralleling to the bedding plane within these facies (Fig. 3(g)). Generally, facies Scb constitutes thick bedded sand units with upward-coarsening sequence, which encased within dark-colored mudstones with sharp upper contacts and located far from coeval deltas.

Interpretation: Typical trough or tabular cross-bedding indicate deposition from traction flows. Discontinuous mud layers in lamina-scales suggested turbulent water conditions, which probably suggest an original river-mouth environment where deposition proceed considering the vertical coarsening trends upward (mouth-bar). A long distance from coeval deltas and located in deep-water areas with interbedded dark-colored muds indicate resedimentation processes. In a summary, the undisturbed and organized bedding structures in facies Scb is interpreted as sandy gravity slides due to their isolated occurrence in deep-water mud, in which sedimentary structures and textures can be well-preserved due to elastic rheology of transported slide blocks (Dott, 1963; Johnson, 1970; Shanmugam, 1996).

4.1.7. Deformed bedded (muddy) sandstone (Sdb)

Description: Facies Sdb is composed of sands with deformed-bedding and internal contorted thin mud layers (Fig. 3(h); Table 1). This facies is characterized by folded sands with folded mud layers (folded heterolithic facies) and minor faults within these sandy units, and generally interbedded with undeformed sandy or muddy units. They generally have an irregular basal contact with underlying dark-colored mudstones, associated sand injection can be occasionally observed in the underlying mudstone.

Interpretation: Folded sandstone interbedded with undeformed sandstone or mudstone is suggested to be the most convincing evidence of syn-depositional deformation in slump sheets (Woodcock, 1976). Sandy slumps from the Eocene North Sea Basin, display folded sands interbedded with undeformed muds and sand injections at the basal shear zone (Shanmugam, 1996). Folded heterolithic facies are widely distinguished as sandy slumps, such as the SE France Annot sandstone, the Paleogene Faeroe Basin, and the Paleocene North Sea (Shanmugam et al., 1995; Shanmugam, 2012). Features of facies Sdb display evidence of syn-depositional deformation and fracture deformation, contorted layers and minor faults in deformed sandy units probably indicate rotational movements and resulted internal fractures. Irregular basal contact can be attributed to the basal shear zone while sliding. In a summary, deformed bedded (muddy) sandstone has been interpreted as deposition by sandy slumps.

4.1.8. Deformed bedded (sandy) mudstone (Mdb)

Description: Facies Mdb consists of gray, dark-gray or black colored, mudstone with deformed bedding (Fig. 3(i); Table 1). This facies is characterized by contorted and elongated sand layers in deformed mud units (folded heterolithic facies) with steep fabrics. This facies is comparable to facies Sdb, regarding to their sedimentary structures. Generally, the surface that separate facies Mdb with underlying and overlying dark-colored deep-water muds is obscure due to the similar color and grain-size.

Interpretation: Muddy slumps have been both reported in modern and ancient deep-marine sediments from mass-movement processes (Plint, 1986; Cronin et al., 2005; Zhang et al., 2016), they can significantly developed in mud-dominated slopes (Galloway, 1998). The deformation structures in facies Mdb can be attribute to rotated muddy slump blocks. Compared to sandy slide blocks, the wriggling-gliding mud-rich blocks can generally hardly preserve their original structures and textures due to high contents of interstitial water. Similar contorted layers have been observed in Pennsylvanian Jackfork Group shale, which has been interpreted as muddy slumps (Shanmugam and Moiola, 1994).

4.1.9. Massive mudstone with floating clasts (Mfc)

Description: Facies Mfc consists of dark gray or black colored, massive mudstones with floating clasts (Fig. 3(j); Table 1). Sand clasts generally show subrounded in shape, while mud clasts generally display subrounded pebbles and rip-ups. Planar or subvertical clast fabrics can be observed.

Interpretation: The grain size of debris flow deposits can vary greatly from clay to large boulders (Coussot and Meunier, 1996; Zhang et al., 2016; Yang et al., 2020). The presence of floating rip-ups with subvertical clast arrangement in mud matrix of facies Mfc (Fig. 3(j)) are unequivocal evidence of plastic flows deposition (Johnson, 1970, 1984; Hiscott and James, 1985; Nemec, 1990; Sohn et al., 1999; Marr et al., 2001) which indicate the thixotropic nature of transporting mediumand suggest clay-rich, cohesive debris flows.

In this area, facies Mfc is attributed to the deposition of mudflows, the definition of which (Sharp and Nobles, 1953) is suggested to be coincident with the range of cohesive debris flows (Lowe, 1979). The concept of mudflow (also called fine muddy debris flows; Coussot and Meunier, 1996) has been widely applied and studied in field observation, core examination and laboratory experiments (Sharp and Nobles, 1953; Li, 1983; Costa and Williams, 1984; O'Brien and Julien, 1988; Whipple and Dunne, 1992; Walsh et al., 2006; Sawyer et al., 2012; Coussot, 2017; Peng, 2021; Peng et al., 2022), the deposits of which are generally characterized by ungraded, poor sorting mud-rock mixture containing large floating clasts or stones (Sharp and Nobles, 1953; Morton and Campbell, 1974) that can be comparable to facies Mfc.

bedded sandstone with underlying normally graded sandstone (**f**); cross bedded sandstone (**g**); deformed bedded muddy sandstone with inter minor faults (**h**); deformed bedded sandy mudstone (**i**); massive mudstone with subrounded floating clasts with planar or subvertical fabrics (**j**); mc: mudclast, sc: sand clast, rc: rafted clast, rf: random fabric, wr: wave ripples, pf: planar fabric.

4.2. Facies associations

Seven broad facies associations can be further recognized by core examination and facies sequence analysis for the nine resedimented facies in the studied interval, including (a) very thick bedded sandy debrites; (b) thick to thin bedded hybrid beds; (c) thick to very thick bedded muddy debrites; (d) very thick bedded mud flow deposits; (e) very thick bedded sandy slides; (f) thick to very thick bedded sandy or muddy slumps; (g) thick to thin bedded turbidites (Fig. 4).

The very thick bedded sandy debrites (~1–3 m) are composed of clean massive sands (Scm) or massive sands with floating clasts (Sfc) (Fig. 4a1-a2). This facies association is typically characterized by amalgamated sand layers. The thick to thin bedded hybrid beds (~0.1–1 m) generally consists of facies from different flow origin. This facies association can display lower massive sands (Sfc/Sc) with fining-up turbidite tops (Swb) (~1 m) (Fig. 4b1), or massive sands (Sfc/Sc) with muddy debrite tops (SMfc) (~1 m) and graded sandstone with overlying rippled sands (Swb) (~0.1–0.5 m) (Fig. 4b2-b3). The thick to very thick bedded muddy debrites (~0.5–5 m) consists of amalgamated muddy sands with floating clasts (MSfc) (Fig. 4(c)), while the very thick bedded mud flow deposits (~1–3 m) consist of amalgamated muds with floating rip-ups (Mfc) (Fig. 4(d)). The very thick bedded sandy slides (~1–1.5 m) are composed of cross-bedded sands with upward-coarsening vertical profiles which generally interbedded with dark-colored laminated muds (Fig. 4(e)). The thick to very thick bedded sandy slumps or muddy slumps (~0.5–3 m) consists of deformed sands (Sdb) or deformed muds (Mdb) without apparent vertical variations in grain-size (Fig. 4(f)). The thick to thin bedded turbidites (~0.1–0.5 m) consists of sands with normal grading (Sng). The units are generally immediately contact with dark-colored lacustrine muds and less than 0.5 m in thick (Fig. 4(g)).

4.3. Facies quantification

Statistic and analyse of the total 968 m of conventional cores reveal the relative importance of different gravity flow types in the $Es3^{m}$ (Fig. 5). Quantitative analysis of facies thicknesses from nine resedimented facies suggests that debrite facies (i.e., facies Scm, Sfc, SMfc, Mfc) account for 81.73% of total thickness, indicate a debris flow domination, while turbidite facies (i.e., facies Sng, Swb), sandy slides (i.e., facies Scb) or slumps (i.e. facies Sdb, Mdb) are less important, which account for 4.55%, 4.82 and 8.9% of total thickness, respectively. Moreover, sandy debrites (facies Scm, Sfc) can account for 42.5% of total thickness (Fig. 5(a)).

Additionally, facies quantification also reveals the relatively contribution of different debris flow types in debrites (Fig. 5(b)). Sandy debrites contribute the largest proportion of 52%, whereas muddy debrites and mudflow deposits account for 22% and 26% in all cored wells, respectively (Fig. 5(b)).

5. Discussion

5.1. Architectural elements, distribution and evolution

5.1.1. Classification and characteristics of deep-water depositional elements

Five different types of deep-water depositional elements have been identified and classified, including slides, slumps, debrite channels, debrite lobes and turbidite sheets, according to their filling patterns, vertical sequences, geometries and morphologies (Table 2), which constitute the fundamental building blocks of the sub-lacustrine debrite systems in the Eocene Dongying deep-basin.

5.1.1.1. Slide masses. Slide masses represent one of the mass-transport deposits (MTDs). They are coherent solid sediment bodies that derived from downslope movement of elastic sediment blocks (high sediment concentration), which represent one of the basic depositional elements in deep-water basins (Galloway, 1998; Stow and Mayall, 2000; Masson et al., 2006). In the Eocene Dongying Rift, slide masses are characterized by lenticular shaped, medium to high-amplitute reflections on seismic profiles, and generally show funnel-shaped or blocky-shaped well-log patterns (Fig. 6(a) and (b); Table 2) with upward-coarsening vertical sequences and traction structures in cores which probably indicate the parental mouth-bar sands (Fig. 6(c)). Typical, the widths and lengths of slide masses range from 2 to 4 km and 2–6 km,

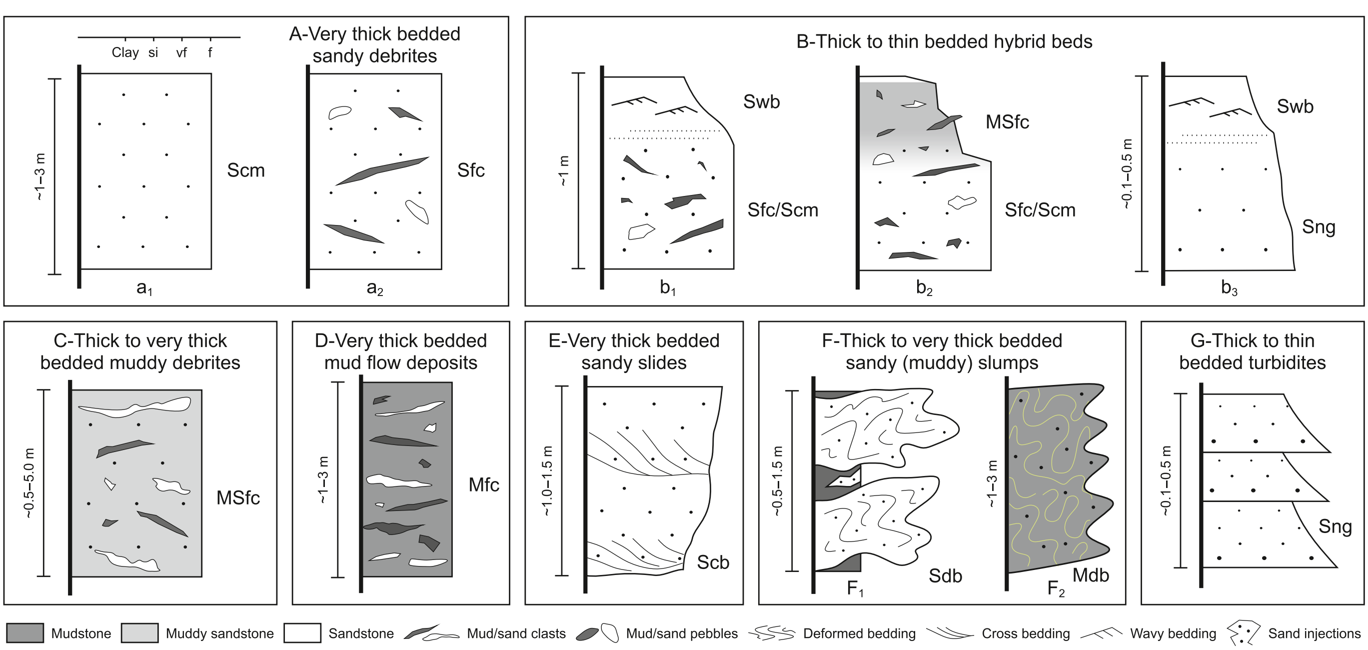

Fig. 4. Facies associations of resedimented deposits, with schematic indications of key features. f: fine sand; vf: very fine sand; si: silt. See the facies code in Table 1.

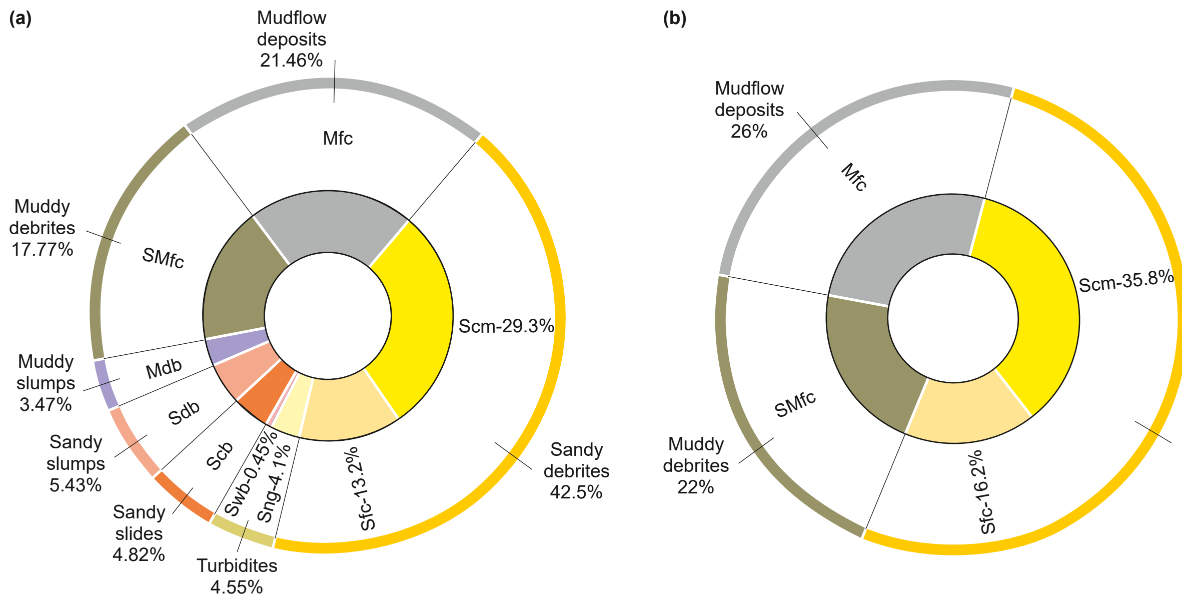

Fig. 5. Facies quantification of the studied interval based on thicknesses of different types of resedimented facies on cored wells. (**a**) Pie chart showing facies proportions based on the total thickness of resedimented facies in all 968 m of cores. (**b**) Pie chart showing debrite facies proportions in the study area. See the facies code in Table 1.

Table 2
Architectural elements of the sub-lacustrine debrite system in the Eocene Dongying Rift.

Depositional element	Filling facies	Process	Features	Scale			
				Thickness, m	Width, km	Length, km	Area, km^2
Slide masses 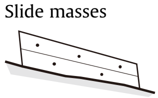	Scb	Sandy slide	Lenticular shaped, medium- to high-amplitute Inverse rhythm sequence or funnel-shaped well-log pattern (mouth bar)	30–150	2–4	2–6	5–20
Slump masses 	Sdb/Mdb	Sandy/muddy slump	Lenticular shaped, chaotic or blank reflections Funnel-shaped or serrated well-log pattern	30–200	2–5	3–6	5–25
Debrite channels 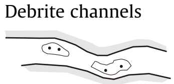	Scm/Sfc/MSfc/Mfc	Debris flowTurbidity currentMudflow	Discontinuous and high-amplitute reflections Blocky-shaped, bell-shaped or irregular well-log pattern	5–40	1–3	>10	–
Debrite lobes 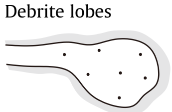	Scm/Sfc/MSfcMfc/Sng/Swc	Debris flowTurbidity currentMudflow	Continuous, parallel and high-amplitute reflection Funnel-shaped, blocky-shaped or irregular well-log pattern	5–35	3–5	5–8	8–30
Turbidite sheets 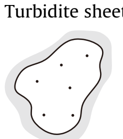	Sng/Swc	Turbidity current	Continuous, parallel and medium-amplitute reflection Irregular or serrated well-log pattern	<0.5	1–4	1–4	2–15

respectively, the thicknesses range from 30 to 150 m, which are much smaller from their submarine cousins (Woodcock, 1976; Masson et al., 2006; Calvès et al., 2015; Soutter et al., 2018). They are commonly sand-rich, partly because it's near impossible to maintain the internal structures and textures in muddy slides during transport due to high water contents, besides, it hard to identify a true 'muddy slide' within deep-water contexts.

5.1.1.2. Slump masses. Slump masses are elastic-plastic sediment blocks with internal deformed sedimentary structures, which suggest longer transport distance and significant liquefaction, compared to slide masses. In the studied interval, slumps are generally lenticular in shape with chaotic or blank seismic facies on seismic profiles, and show funnel or serrated log motifs. The widths and lengths range from 2 to 5 and 3–6 km and thicknesses is less than 200 m (Fig. 7; Table 2). These sediment masses can be sand-rich or mud-rich, filled by deformed sand facies (Sdb) or deformed mud facies (Mdb) which constitute sandy slump masses and mud slump masses, respectively.

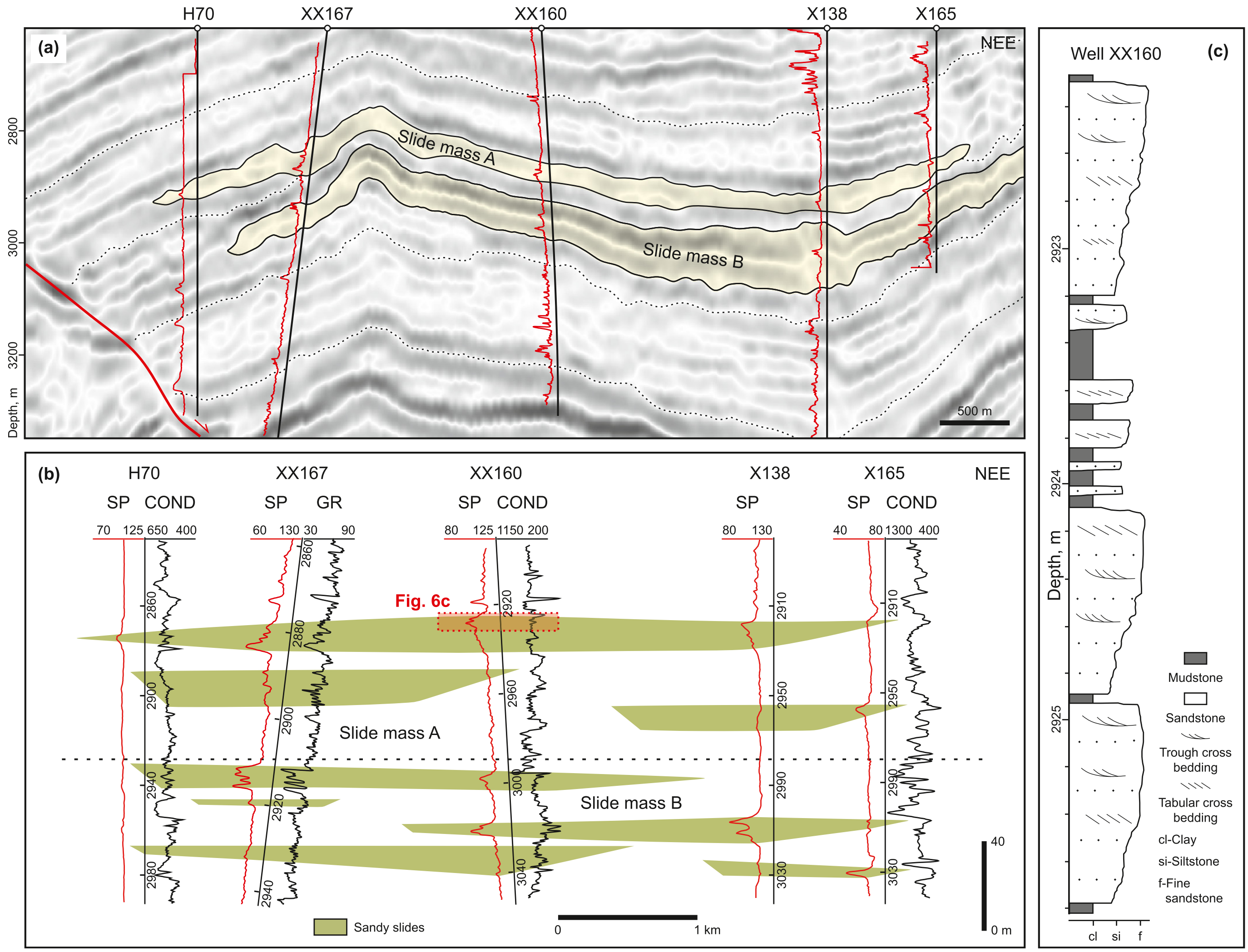

Fig. 6. Well-tied transverse seismic profile across slide masses showing medium to high amplitude reflections, displayed well logs are spontaneous potential curves (**a**); borehole correlation profiles showing sand distribution of sandy masses (**b**); and sand beds in sandy masses commonly display inverse grain-size rhythms (**c**). SP: spontaneous potential; GR: gamma ray; COND: conductivity. See Fig. 1 for the line location.

5.1.1.3. Debrite channels. Debrite channels constitute the main conduit that transport gravity flows and sediments into the deep lake in debrite system in the study area. Generally, they display discontinuous and high-amplitute reflections on seismic profiles. Their width ranges from 1 km to less than 3 km, and their lengths are generally larger than 10 km, while thicknesses are less than 40 m (Table 2). They are dominated by sandy or muddy debris flows rather than turbidity currents. Additionally, sandy debrite channels are typically distributed in the proximal delta-slopes and characterized by Scm and Sfc facies with blocky (Fig. 8(a)) or bell-shaped (Fig. 8(b)) log patterns, while muddy debrite channels are more basin-ward located and show irregular or serrated log patterns which are mainly filled by facies MSfc or Mfc. (Fig. 8(c)).

5.1.1.4. Debrite lobes. Debrite lobes represent spatially localized accumulation of debrites found at the downstream end of debrite channel. These lobes commonly display high-amplitute reflections on seismic profiles and show funnel-shaped or blocky-shaped well-log patterns which probably record focused aggradation or progradation of sediment while channelized debris flows deceleration and spread (Shanmugam, 2016; Liu et al., 2017) (Fig. 9(a) and (b); Table 2). Areal dimension is variable, but usually extend up to 5–8 km with the largest thickness of approximately 35 m, suggest an unusual high aspect ratio (i.e. width to maximum thickness) of approximately 150:1 (Fig. 9(c)(e)), whereas the measurements of aspect ratio from turbidite lobes in marine settings are nearly 1000:1 (Prélat et al., 2010; Koo et al., 2016), which can be attributed to the plastic rheology and 'en masse' deposition of debris flows. Debrite lobes can be sand or mud-rich and generally consist of amalgamated fine-grained sandy debrites (Scm, Sfc) or muddy debrites (MSfc) (Fig. 9(c)). Thin-bedded turbidites can be found in distal lobe fringe environments.

5.1.1.5. Turbidite sheets. Turbidite sheets are composed of deposits from deposition of low density turbidity currents. They display thin bedded sands with thicknesses usually less than 0.5 m, while their width and length can reach as large as several kilometers. They display continuous, parallel, and strong-to medium-amplitute on seismic profiles (Hackbarth and Shaw, 1994; Posamentier and Kolla, 2003) with irregular or serrated log patterns, and fining-up sequences (Fig. 10; Table 2). They commonly located in front of debrite lobes or the lateral margins of debrite channels due to sediment unload or channel overflows.

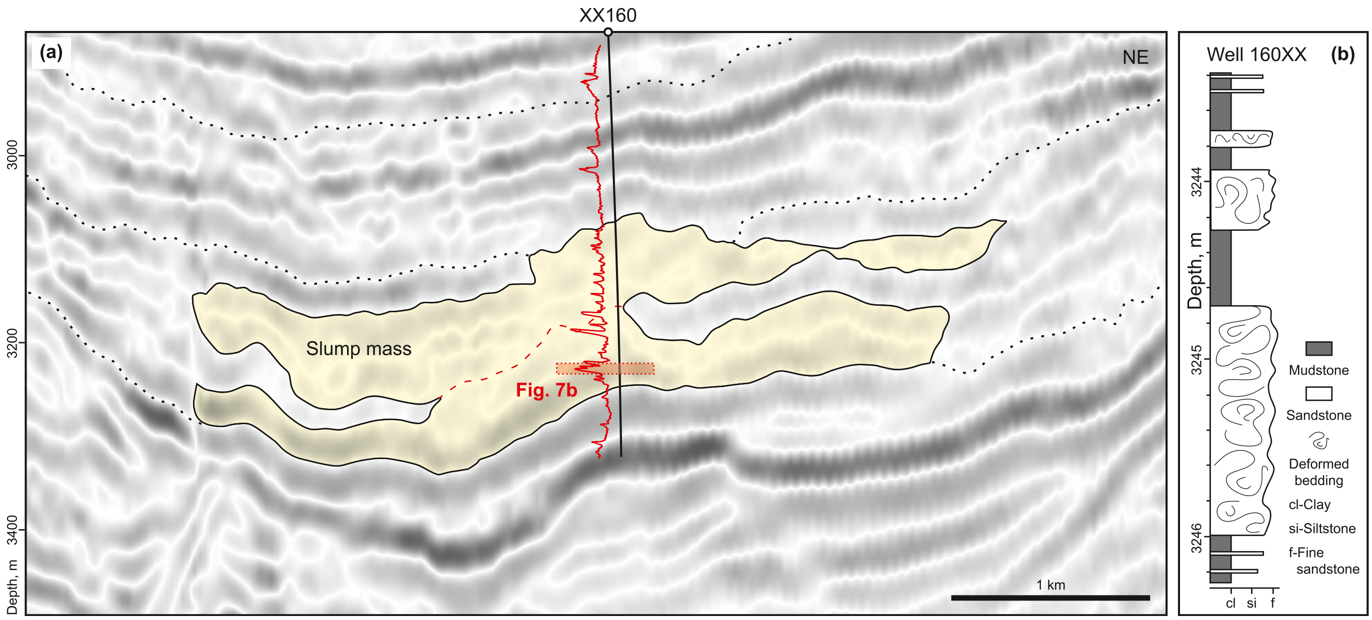

Fig. 7. Well-tied transverse seismic profile across slump masses showing chaotic and blank amplitude reflections, well logs displayed are spontaneous potential curves (**a**); and deformed beddings are typical observed within these slump beds (**b**). See Fig. 1 for the line location.

5.1.2. Co-evolution of the deep debrite system and lacustrine delta

The Eocene sub-lacustrine debrite system has been revealed by utilization of seismic imaging to better understand the planar facies arrangement and distribution. The debrite system was well-documented in correlation with the development of coeval Dongying Delta (Figs. 11 and 12). Slide or slump masses distributed along the progradation direction of the adjoining delta-front, whereas debrite channels, lobes and turbidite sheets located forward ahead these sediment blocks. Additionally, the planar distribution of debrite lobes show significant correlation with local syn-depositional faults, which generally developed in down-dropped blocks (Fig. 11). Moreover, the studied interval, which is generally subdivided into six sand groups (i.e. parasequence sets; PSS) is characterized by six phases of continuously prograding delta-debrite system during the whole $Es3^m$ (Fig. 12).

5.2. Deep-lacustrine flow process initiated from delta-slope failure

Slope failure and resulting landslides have been extensively studied and are considered the dominant mechanism for significant sediment accumulation in modern deep-sea environments (Talling et al., 2007; and the review on sediment gravity flows by Talling, 2014), which can promote the formation of slides, slumps, debris flows and turbidity currents successively (Shanmugam, 2000, 2012). Five broad types of subaqueous gravity-driven processes, including slide (sandy), slump (sandy and muddy), debris flow (sandy and muddy), mudflow and turbidity current have been recognized in the Eocene Dongying Rift based on facies identification and interpretation, and flow rheology analysis (Table 1; Fig. 3). These processes can be attributed to the triggering by Dongying Delta-slope failures. Furthermore, the organized distribution of deep-water elements from slide or slump masses to debrite channels, lobes, and turbidite sheets along the delta-progradation direction suggests a coherent transport process from slide, slump, debris flow to turbidity current (Fig. 13). The instability of older sediments is a prerequisite for slope failure and subsequent sediment gravity flow generation. Strong sediment supply is commonly regarded as a primary driver of instability on the delta-front slope, promoting sediment failure and concomitant slump-derived gravity flows (Coleman and Prior, 1982; Hampton et al., 1996). Based on the calculation of the distribution and thickness of the Dongying delta, Li (2005) proposed that during the delta progradation, the sediment flux can reach up to nearly 1.6×10^{11} m^3 (Li, 2005), resulted in an average progradation rate of around 20 km/Myr (Qiu et al., 2001). Additionally, earthquakes induced by fault movements are important trigger for slope failure and deep-water gravity flows initiation (Shepard, 1932; Heezen and Ewing, 1952). According to the previous studies, the frequent activities of the border fault led to a very high subsidence rate of 300–500 m/Myr during the deposition of the Eocene Shahejie Formation in the Dongying rift (Feng et al., 2013). Considering the high sediment accumulation rate in the delta-front and intense tectonic movements, it is proposed that active fault movement combined with depositional loading plays a pivotal role in slope failures and sediment gravity flow generation.

In addition, the examination of the core and analysis of facies indicate a significant vertical facies connection between lower sandy debrite and overlying muddy debrite or turbidite. This connection probably represents successive gravity flow events (Fig. 4b1-b3). Architectural element analysis further suggests that sandy debrite channels generally develop in proximal slope areas, while muddy debrite channels are located in distal basin-floor areas, and thin bedded turbidite sheets increase in lobe fringes or lateral channel margins (Figs. 8 and 10). Therefore, it is suggested that sandy debris flow can gradually transform into muddy debris flow and turbidity current during transport. Linked muddy debrites are likely the result of powerful sandy debris flow eroding the sea floor, incorporating mud and increasing the mud matrix, turning into viscous muddy debris flow (Liu et al., 2017), and then deposit due to the decrease of flow velocity at the distal basin floor with more gentle topography gradient (Peng, 2021). The mechanism proposed to interpret the existence of clay-rich debris flow in high-density turbidity currents (Haughton et al., 2003; Talling et al., 2004; Kane et al., 2017). Hydroplaning at the base of cohesive and clay-rich gravity flow in deep-water settings can prevent large-scale erosion because of reduced flow resistance at the seafloor/

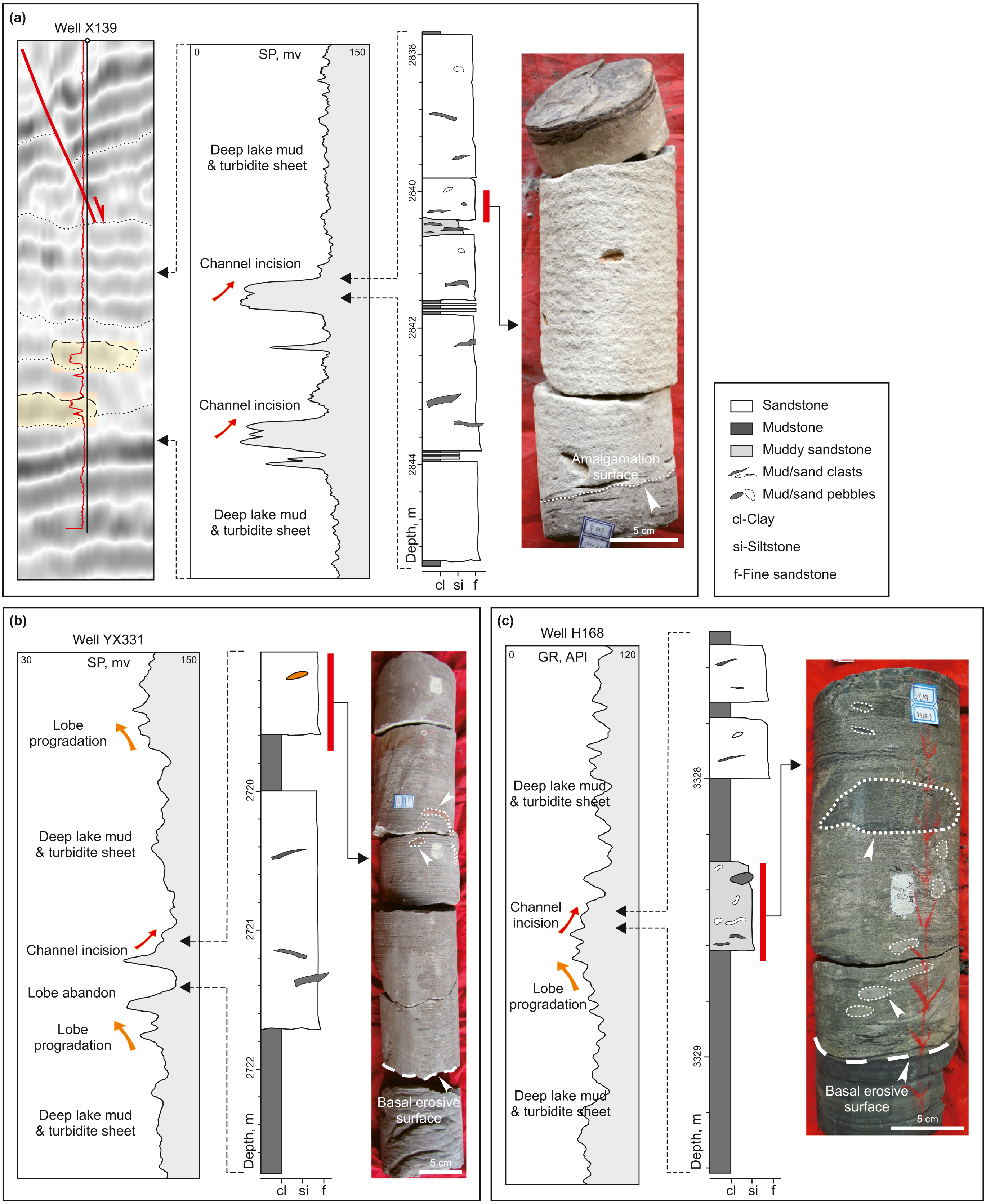

Fig. 8. Blocky or bell-shaped logging patterns and filling types of sandy debrite channel (**a**–**b**) and muddy debrite channel (**c**). SP: spontaneous potential; GR: gamma ray. See Fig. 1 for the well locations.

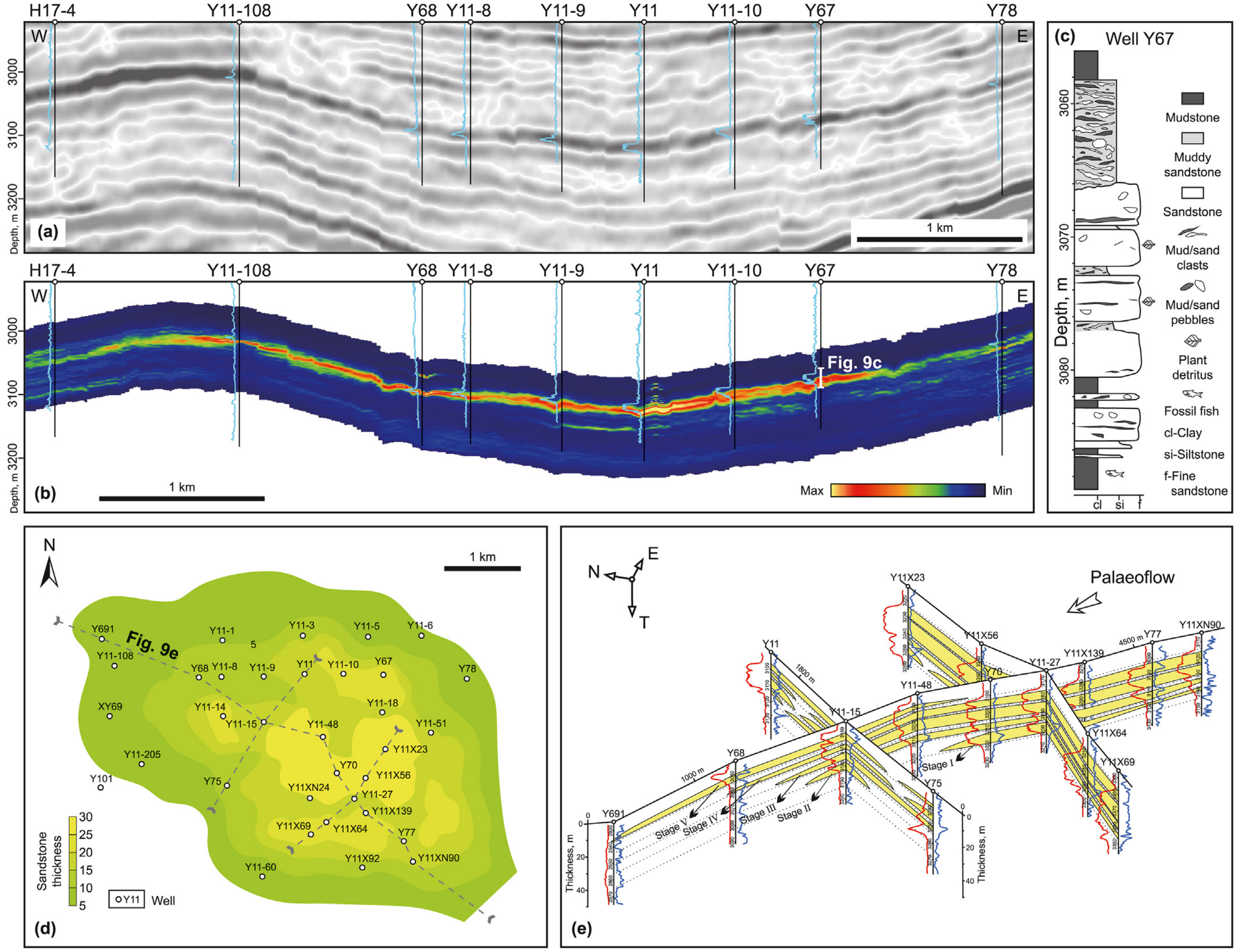

Fig. 9. Well-tied seismic profile along depositional-dip illustrating the strong amplitude reflections of debrite lobe (**a**); sandstone inversion profile showing sand distribution in the WE direction (**b**); cored well revealing amalgamated sandy and muddy debrites constituting the lobe (**c**); sandstone thickness map of the debrite lobe (**d**); and three-dimensional diagram showing multiple stages of debrite lobe grow (**e**) (modified from Liu et al., 2017). Well logs displayed are spontaneous potential curves. See Fig. 1 for the line location.

flow interface (Fig. 13). However, non-cohesive and sand-rich debris flow can hardly hydroplane due to extremely low cohesive strength and high permeability (Sohn, 2000; Mulder and Alexander, 2001), which may lead to significant seafloor erosion. Historical events demonstrate that during the process of submarine landsliding to debris flow and turbidity current, the final deposits volume can reach several times the sediment volume from the initial slope failure, which suggests the importance of seafloor erosion in gravity flow deposition (Piper and Aksu, 1987; Nisbet and Piper, 1998). Accordingly, in the Dongying Rift, muddy debris flow is probably generated from erosional sandy debris flow through the increasing of mud matrix and viscous strength during transport. This would explain the emplacement of floating muddy rip-ups in sandy debrite as well as the dark-gray colored muddy-sand matrix in muddy debrite (Fig. 3(b) and (c)).

Turbidity current generation from the transformation of debris flow has been widely documented in world deep-water basins and in experimental studies, and commonly occur due to increased fluid contents (Fisher, 1983; Mohrig et al., 1998; Felix and Peakall, 2006; 2009; Talling et al., 2012; Zou et al., 2012). Dilution or mixing by penetration of water into the interior of debris flows through clefts along the flow-fronts, disintegration and detachment of hydroplaning flow-fronts, and hydraulic jump at slope breaks or entrainment of the upper flow body can produce turbidity currents (Allen, 1971; Fisher, 1983; Weirich, 1988; Lee et al., 1999; Parsons et al., 2001). Previously studies suggest that cohesive debris flow can more easily transform into low-density subsidiary turbidity current because of the high mobility of hydroplaning flow-front in contrast to non-cohesive, sandy debris flow (Mohrig et al., 1998). Generally, a completely gravity-driven process consists of landslide, slump, debris flow and turbidity current, can sequentially occur along the transport paths (Shanmugam et al., 1994).

However, compared to the traditional and widely reported turbidite systems (Mutti et al., 2009), the studied sub-lacustrine system is characterized by poorly developed turbidites (account for <9% in total thickness) with widespread debrites (account for 80% in total thickness), which probably indicate a limited transformation from debris flow into turbidity current, and coincide with the flume observation of the inefficient conversion from debris flow into dilute turbidite current (Maar, 1999) and the outcrop examination that large-scale debris flows tend to produce relatively small turbidites (Plink-Björklund and Steel, 2004). Additionally, it is documented that debris flow can travel hundreds of kilometers along the modern seafloor without undergoing

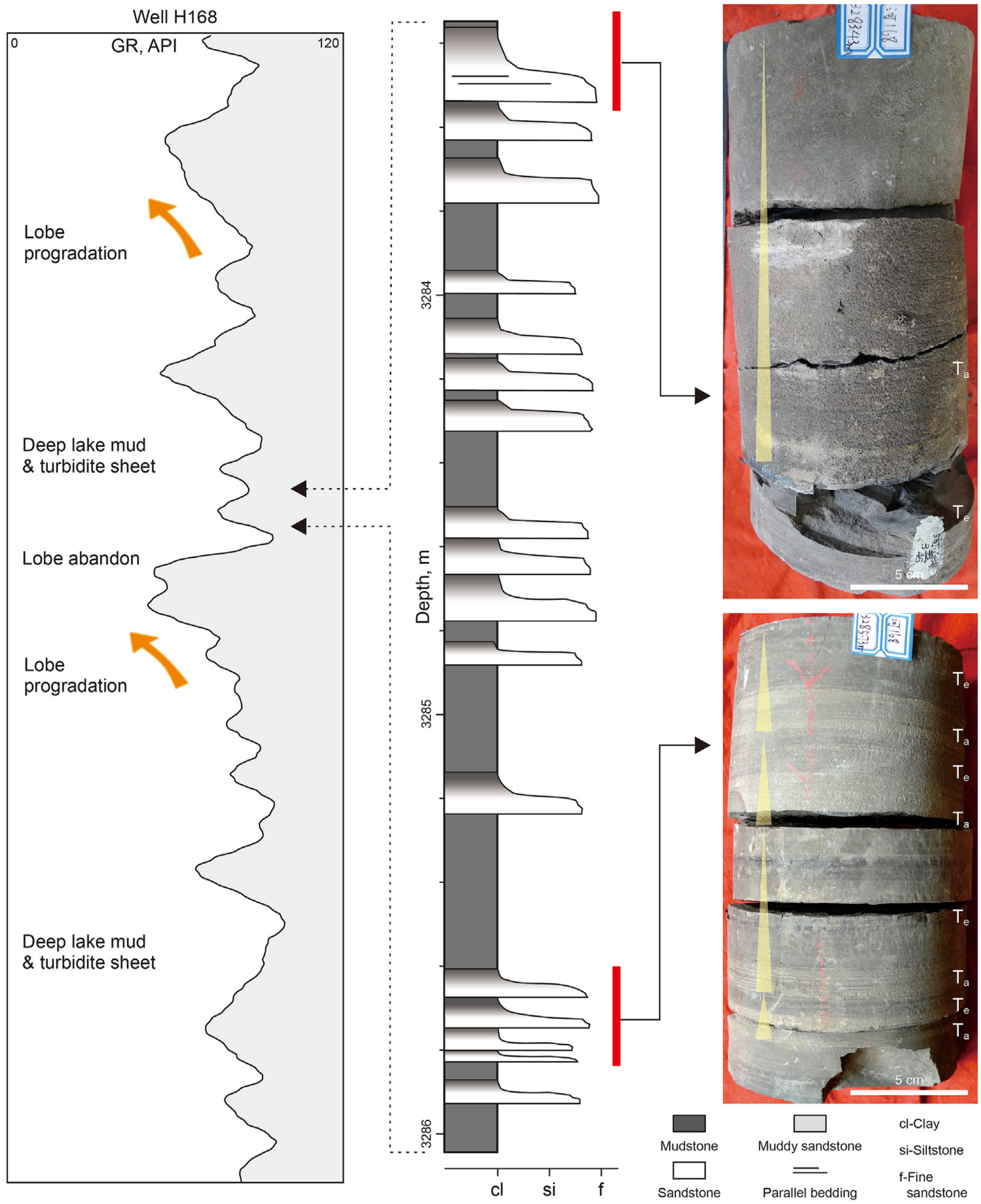

Fig. 10. Well logging patterns and cored well revealing filling facies of turbidite sheets. See Fig. 1 for the well location.

significant dilution (Gee et al., 1999; Piper et al., 1999; Masson et al., 2006), while those deep rift depocenters of lacustrine basins are generally characterized by short transport distances (Lawton, 2019), in which the dilution and conversion of gravity flows are probably restricted due to insufficient transportation. In the Eocene Dongying Rift, the transport distance of gravity flows from the delta-front to the deep-basin is approximately 10 km which is dominated by the local topography related with syn-depositional faults (Fig. 1(c)–(e)). Moreover, the observed resedimented facies suggest two types of deep-water process, depending on the initial composition of the failed sediments, sandy slide can convert into sandy slump, sandy debris flow, muddy debris flow and turbidity current, while mud flow can generate from mud slumps.

5.3. Sediment distribution pattern of sub-lacustrine debrite system and implications for deep-water exploration

Turbidite systems in deep-lacustrine rift basins can vary greatly from their marine counterparts due to different basin morphology, tectonic activity and depositional process. The delivery mechanism, whether it is turbidity currents, debris flows, slump, slide, etc., plays a significant role in determining deep-water architectural element types and their dispersal patterns (Mutti and Normark, 1991; Posamentier and Kolla, 2003). Architectural elements in the Eocene Dongying Rift show good correlation with depositional processes and flow transformation. The well-developed and dominated debris flows or slides, slumps contribute the basic types of facies building blocks, while turbidites are less important in forming sub-lacustrine systems. In addition, fault movements are suggested as an important factor controlling the formation and distribution of debrite system. Activities of syn-depositional faults generally lead to local adjustment in basin topography, which play an important role in sediment transport and deposition in turn (Gawthorpe and Leeder, 2000; Lin et al., 2000; Muravchik et al., 2020). In the Dongying Rift, gravity flow deposits generally formed immediately down-dip of the syn-depositional faults, the

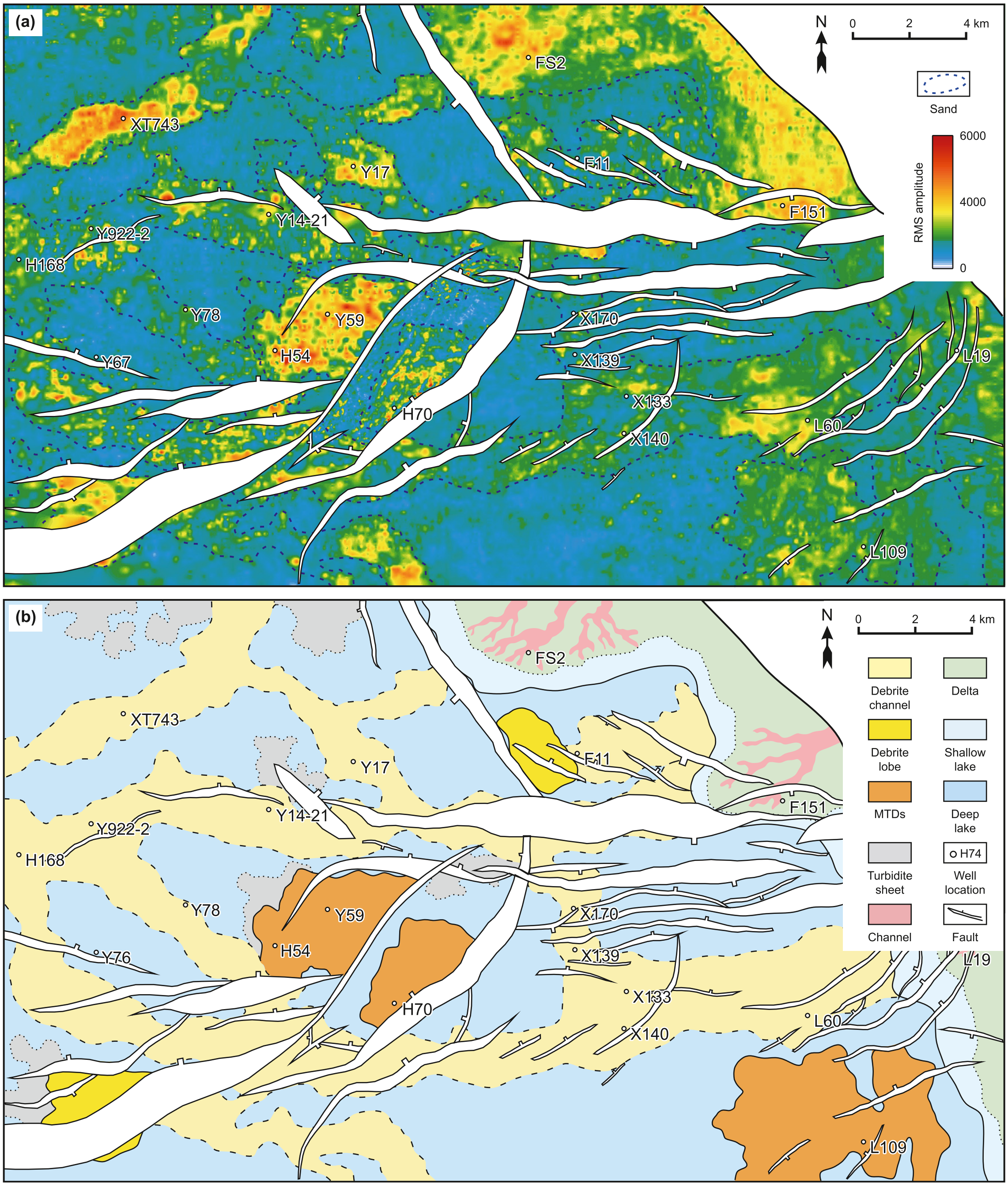

Fig. 11. Stratal slice through sub-lacustrine debrite system and coeval deltas illustrating planar arrangements of deep-water elements.

lobes mainly occur in local topographic lows which are laterally confined by syn-depositional faults (Feng et al., 2016). Results from this study demonstrate that the extension and dispersal of debrite lobes and channels are well correlated with fault distribution (Fig. 11), which suggest fault activities have important influences on local sediment differentiation and accumulations.

Resultantly, a depositional model is proposed to depict the sub-lacustrine debrite system in the Dongying Delta-slope setting in the Eocene Dongying Rift, which highlights the interaction between depositional setting, flow process and basin architecture (Fig. 14). Sandy slides, sandy slumps and muddy slumps are commonly developed on the sub-lacustrine lobes in adjacent to delta-fronts, while mud flow deposits may occur downslope as muddy slumps continually transport (Fig. 14(a)), and sandy debrite channels, muddy debrite channels, muddy debrite lobes and turbidite sheets can occur successively along the depositional direction after sufficient transportation and transformation (Fig. 14(b)). When fault activities were significant, sediments can rest in proximal topographic lows controlled by syn-depositional faults, and muddy debrite dominated channels and lobes may not occur due to limited flow transformation (Fig. 14(c)).

The deep-water system under consideration is characterized by the prevalence of debris flows, as opposed to turbidity currents. This distinction is significant in terms of the depositional process, facies architecture, and dispersal pattern when compared to the classic deep-marine turbidite system (Normark, 1970; Walker,

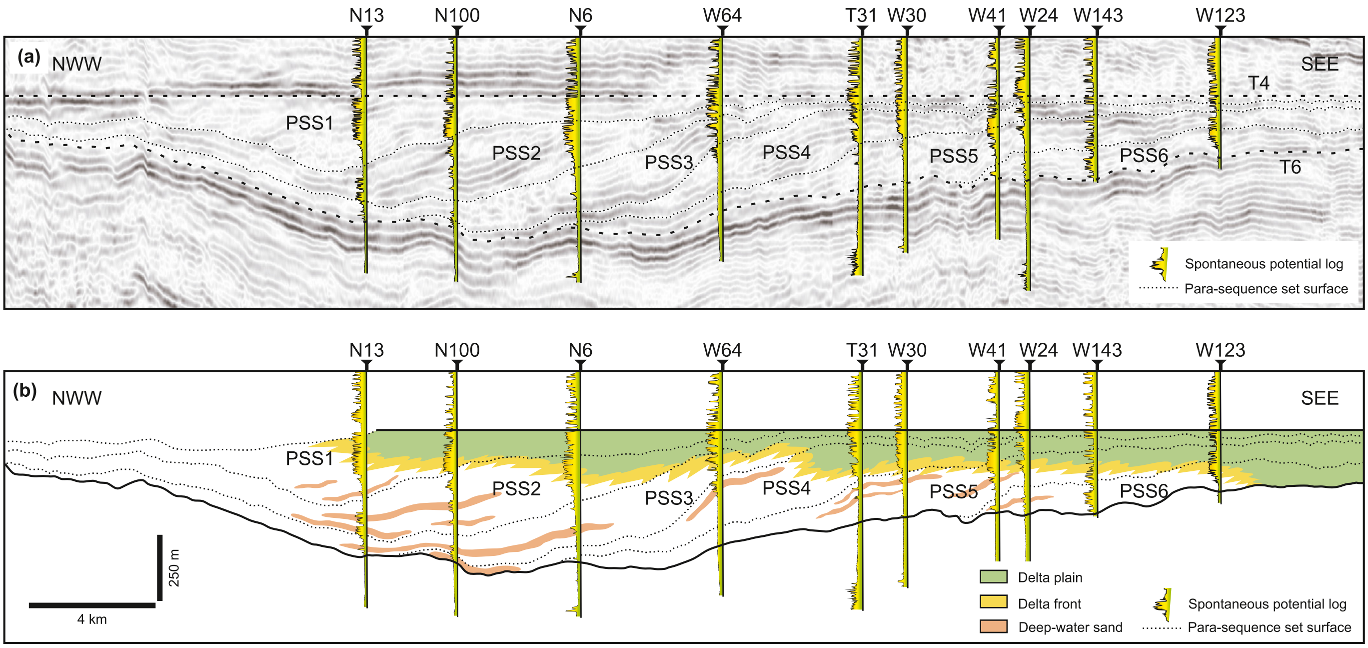

Fig. 12. Depositional dip-orientated seismic profile (flattened to ancient delta plain surface T4) (**a**) and interpreted seismic profile indicating multiple progradation and distribution of delta-debrite system during the deposition of the $Es3^m$ in the Dongying Rift (**b**).

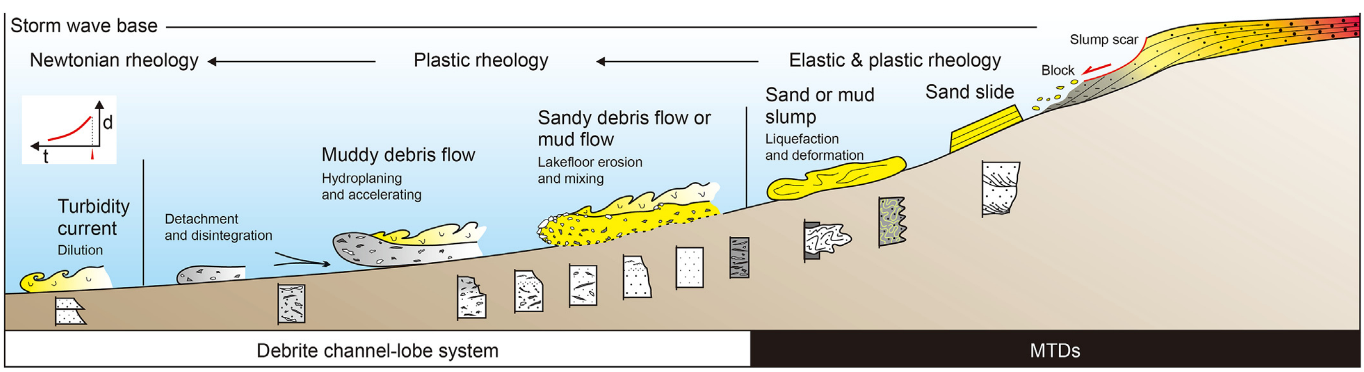

Fig. 13. Idealized sedimentary process illustrates the transportation and transformation of sediment gravity flows in delta-failure-controlled deep-lacustrine slopes.

1978; Reading and Richards, 1994; Posamentier and Kolla, 2003; Prélat et al., 2009). The sub-lacustrine debrite system described herein can represent a typical example of deep-water deposition in lacustrine rift basins. A detailed examination of the depositional process, facies architecture, and dispersal pattern of this deep-water system can provide novel insights into the diversity of deep-water deposition in deep-water basins worldwide.

In addition, the proposed model has the potential to be utilized in predicting reservoirs for debrite-dominated systems in deep-water basins across the globe. The Eocene Dongying Rift has confirmed that sandy debrite channels, lobes, and sandy slide masses are significant pay zones. Sandy debrite channels and lobes consist of massive sands with higher porosity and permeability compared to muddy debrites, mudflow deposits, slumps, or turbidites due to their larger grain size, better sorting, and lower mud content. Furthermore, sandy debrite is the most extensively developed facies in the studied section, as determined by facies quantification. Sandy slide masses inherit their properties from parental deltaic sands due to well-preserved textures and structures. Although they are not as widely distributed as channels or lobes in debrite-dominated systems, they generally have greater thicknesses. Sandy debrite lobes, in particular, have higher aspect ratios than turbidite lobes, indicating that they likely have considerable thicknesses in small areas. Additionally, The physical property test data show that the porosity of sandy debrite lobes can reach 17–27%, with permeability ranging from approximately 10–581 millidarcies. In the Dongying Depression, the oil-bearing area of a single sandy debrite lobe reservoir can exceed 10 km^2, with an average effective oil layer thickness of over 10 m. The petroleum reserves can exceed tens of millions of tons of oil equivalent (Tian, 2004). On a plan view, the distribution of sandy debrite lobe is controlled by growth fault activities. Sandy debris flows typically unload to form lobes within the space beneath the downthrown block of growth faults, which are also favorable exploration areas for debrite lobe reservoirs (Liu et al., 2017). These depositional elements are typically enclosed within dark-colored source rocks, resulting in efficient hydrocarbon accumulation.

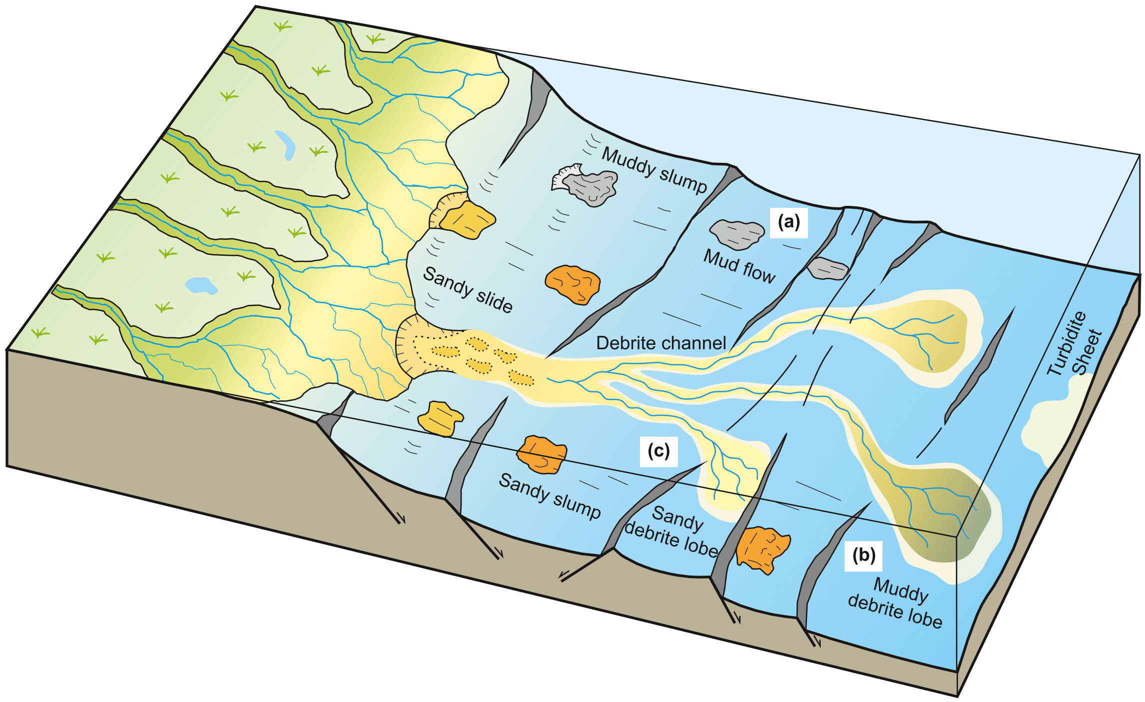

Fig. 14. Depositional model of a sub-lacustrine debrite system in a delta-slope setting in a rift basin.

6. Conclusions

A debrite-dominated sub-lacustrine depositional system has been investigated and documented by an integrated study of well data and seismic data in the Eocene Dongying deep rift basin. The sub-lacustrine system was characterized by nine types of resedimented facies, indicating seven different origins, including sandy slide, sandy slump, sandy debris flow, muddy debris flow, muddy slump, mudflow, and turbidity current, based on core examination, facies sequence and flow rheology analysis. Facies quantification suggest that the system is dominated by debrites, accounting for nearly 82% of the total thickness, rather than slides, slumps, or turbidites. It is proposed that delta-slope failure, combined with frequent fault activities, are the main triggers for gravity flows initiation. Sandy slides can transform into sandy slumps, sandy debris flows, muddy debris flows, and turbidity currents due to liquefaction, deformation, lake-floor erosion, mixing, disintegration, and dilution during transport, and mudflows can result from the liquefaction of muddy slumps.

The depositional characteristics of architectural elements are closely linked to the gravity flow process and include their styles, geometries, distribution, and filling patterns. Based on seismic reflection characteristics, logging, and core facies, five distinct types of architectural elements can be identified and classified. These elements are considered the primary building blocks of sub-lacustrine debrite systems and include (sandy) slide masses, (sandy/muddy) slump masses, (sandy/muddy) debrite channels, (sandy/muddy) debrite lobes, and turbidite sheets. In the study area, sandy debrite channels, lobes, and sandy slide masses are the primary deep-water hydrocarbon reservoirs, while other depositional elements are less significant in forming effective petroleum reservoirs. These findings could be applied to lithologic reservoir exploration in other deep-water basins worldwide with similar geological backgrounds.

CRediT authorship contribution statement

Jian-Ping Liu: Visualization, Validation, Methodology, Investigation. **Ben-Zhong Xian:** Supervision, Resources, Project administration, Conceptualization. **Xian-Feng Tan:** Supervision, Resources, Project administration, Investigation. **Zhen Wang:** Methodology, Investigation, Formal analysis. **Jun-Hui Wang:** Investigation, Formal analysis, Conceptualization. **Long Luo:** Investigation, Methodology, Visualization. **Peng Chen:** Investigation, Formal analysis, Visualization. **Yan-Xin He:** Investigation, Formal analysis, Methodology. **Rong-Heng Tian:** Investigation, Formal analysis, Software. **Qian-Ran Wu:** Visualization, Methodology, Investigation. **Jia Wang:** Software, Visualization, Writing – review & editing. **Jin Li:** Visualization, Software. **Long Chen:** Data curation. **Wen-Yi Peng:** Data curation. **Yi-Man Zhou:** Software. **Quan-Feng Jiang:** Software.

Acknowledgements

We extend our heartfelt gratitude to Professor Liang Chao and the other four anonymous reviewers for their meticulous review, insightful feedback, and invaluable support that have substantially enhanced the quality of this manuscript. We also acknowledge the Shengli Oil Company, Sinopec Group, for providing us with valuable data and technical expertise. This work is supported by the National Natural Science Foundation of China (No. 42202170, 42172109, 42072140, 42102133, 42202122), the Natural Science Foundation of Chongqing (CSTB2022NSCQ-MSX1166, CSTB2022NSCQ-JQX0031), the Science and Technology Research Program of Chongqing Municipal Education Commission (KJQN202201511, KJZD-M202101502) and Project of Chongqing University of Science & Technology (ckrc2022028, YKJCX2320109).

References

Allen, J.R.L., 1971. Mixing at turbidity current heads, and its geological implications. J. Sediment. Res. 41, 97–113. https://doi.org/10.1306/74D721F8-2B21-11D7-

8648000102C1865D.
Amy, L.A., Talling, P.J., Peakall, J., Wynn, R.B., Thynne, R.A., 2005. Bed geometry used to test recognition criteria of turbidites and (sandy) debrites. Sediment. Geol. 179, 163–174. https://doi.org/10.1016/j.sedgeo.2005.04.007.
Bailey, L.P., Clare, M.A., Rosenberger, K.J., Cartigny, M.J.B., Talling, P.J., Paull, C.K., Gwiazda, R., Parsons, D.R., Simmons, S.M., Xu, J., Haigh, I.D., Maier, K.L., McGann, M., Lundsten, E., 2021. Preconditioning by sediment accumulation can produce powerful turbidity currents without major external triggers. Earth Planet Sc Lett 562, 116845. https://doi.org/10.1016/j.epsl.2021.116845.
Bouma, A.H., 1962. Sedimentology of Some Flysch Deposits: A Graphic Approach to Facies Interpretation. Elsevier, Amsterdam, p. 168.
Calvès, G., Huuse, M., Clift, P.D., Brusset, S., 2015. Giant fossil mass wasting off the coast of West India: the Nataraja submarine slide. Earth Planet Sc Lett 432, 265–272. https://doi.org/10.1016/j.epsl.2015.10.022.
Cao, Y.C., Wang, Y.Z., Gluyas, J.G., Liu, H.M., Liu, H.N., Song, M.S., 2018. Depositional model for lacustrine nearshore subaqueous fans in a rift basin: the Eocene Shahejie Formation, dongying sag, Bohai Bay Basin, China. Sedimentology 65, 2117–2148. https://doi.org/10.1111/sed.12459.
Cao, Y.C., Jin, J.H., Liu, H.N., Yang, T., Liu, K.Y., Wang, Y.Z., Wang, J., Liang, C., 2021. Deep-water gravity flow deposits in a lacustrine rift basin and their oil and gas geological significance in eastern China. Petrol. Explor. Dev. 48, 286–298. https://doi.org/10.1016/S1876-3804(21)60023-X.
Chen, P., Xian, B.Z., Li, M.J., Liang, X.W., Wu, Q.R., Zhang, W.M., Wang, J.H., Wang, Z., Liu, J.P., 2021. A giant lacustrine flood-related turbidite system in the Triassic Ordos Basin, China: sedimentary processes and depositional architecture. Sedimentology 68, 3279–3306. https://doi.org/10.1111/sed.12891.
Chen, P., Xian, B.Z., Li, M.J., Fang, L.H., Rahman, N.U., Liu, J.P., Chen, S.R., Tian, R.H., Wu, Q.R., 2023. Intensified lacustrine turbidite deposition as a response to the carnian pluvial episode: insights from the triassic ordos basin in north China plate. Palaeogeogr Palaeocl 111599. https://doi.org/10.1016/j.palaeo.2023.111599.
Coleman, J.M., Prior, D.B., 1982. Deltaic environments of deposition. In: Scholle, P.A., Spearing, D. (Eds.), Sandstone Depositional Environments, vol. 31. AAPG Mere., pp. 139–178
Costa, J.E., Williams, G.P., 1984. Debris-flow Dynamics (Videotape), 84–606. USGS Open-File, 22.5min.
Coussot, P., 2017. Mudflow Rheology and Dynamics. Routledge.
Coussot, P., Meunier, M., 1996. Recognition, classification and mechanical description of debris flows. Earth Sci. Rev. 40, 209–227. https://doi.org/10.1016/0012-8252(95)00065-8.
Cronin, B., Owen, D., Hartley, A., Kneller, B., 1998. Slumps, debris flows and sandy deep-water channel systems: implications for the application of sequence stratigraphy to deep water clastic sediments. J Geol Soc London 155, 429–432. https://doi.org/10.1144/gsjgs.155.3.0429.
Cronin, B.T., Çelik, H., Hurst, A., Turkmen, I., 2005. Mud Prone Entrenched Deep-Water Slope Channel Complexes from the Eocene of Eastern Turkey, vol. 244. Geological Society, London, Special Publications, pp. 155–180. https://doi.org/10.1144/GSL.SP.2005.244.01.1.
Dasgupta, P., 2003. Sediment gravity flow-the conceptual problems. Earth Sci. Rev. 62, 265–281. https://doi.org/10.1016/S0012-8252(02)00160-5.
Dodd, T.J., McCarthy, D.J., Amy, L., Plenderleith, G.E., Clarke, S.M., 2022. Hybrid event bed character and distribution in the context of ancient deep-lacustrine fan models. Sedimentology 69 (4), 1891–1926. https://doi.org/10.1111/sed.12979.
Dott, Jr.R.H., 1963. Dynamics of subaqueous gravity depositional processes. AAPG Bull. 47, 104–128. https://doi.org/10.1306/BC743973-16BE-11D7-8645000102C1865D.
Ducassou, E., Fournier, L., Sierro, F.J., Zarikian, C.A., Lofi, J., Flores, J.A., Roque, C., 2016. Origin of the large Pliocene and Pleistocene debris flows on the Algarve margin. Mar. Geol. 377, 58–76. https://doi.org/10.1016/j.margeo.2015.08.018.
Elverhøi, A., Norem, H., Andersen, E.S., Dowdeswell, J.A., Fossen, I., Haflidason, H., Kenyon, N.H., Laberg, J.S., King, E.L., Sejrup, H.P., Solheim, A., Vorren, T., 1997. On the origin and flow behavior of submarine slides on deep-sea fans along the Norwegian-Barents Sea continental margin. Geo Mar. Lett. 17, 119–125. https://doi.org/10.1007/s003670050016.
Enos, P., 1977. Flow regimes in debris flow. Sedimentology 24, 133–142. https://doi.org/10.1111/j.1365-3091.1977.tb00123.x.
Falk, P.D., Dorsey, R.J., 1998. Rapid development of gravelly high-density turbidity currents in marine Gilbert-type fan deltas, Loreto Basin, Baja California Sur, Mexico. Sedimentology 45, 331–349. https://doi.org/10.1046/j.1365-3091.1998.0153e.x.
Felix, M., Peakall, J., 2006. Transformation of debris flows into turbidity currents: mechanisms inferred from laboratory experiments. Sedimentology 53, 107–123. https://doi.org/10.1111/j.1365-3091.2005.00757.x.
Felix, M., Leszczyński, S., Ślączka, A., Uchman, A., Amy, L., Peakall, J., 2009. Field expressions of the transformation of debris flows into turbidity currents, with examples from the Polish Carpathians and the French Maritime Alps. Mar. Petrol. Geol. 26, 2011–2020. https://doi.org/10.1016/j.marpetgeo.2009.02.014.
Feng, Y.L., Li, S.T., Lu, Y.C., 2013. Sequence stratigraphy and architectural variability in late Eocene lacustrine strata of the Dongying Rift, Bohai Bay Basin, eastern China. Sediment. Geol. 295, 1–26. https://doi.org/10.1016/j.sedgeo.2013.07.004.
Feng, Y.L., Jiang, S., Hu, S.Y., Li, S.T., Lin, C.S., Xie, X.N., 2016. Sequence stratigraphy and importance of syndepositional structural slope-break for architecture of Paleogene syn-rift lacustrine strata, Bohai Bay Basin, E. China. Mar. Petrol. Geol. 69, 183–204. https://doi.org/10.1016/j.marpetgeo.2015.10.013.
Fisher, R.V., 1971. Features of coarse-grained, high-concentration fluids and their deposits. J. Sediment. Res. 41, 916–927. https://doi.org/10.1306/74D723B5-2B21-11D7-8648000102C1865D.
Fisher, R.V., 1983. Flow transformations in sediment gravity flows. Geology 11, 273–274. https://doi.org/10.1130/0091-7613(1983)112.0.CO;2.
Galloway, W.E., 1998. Siliciclastic slope and base-of-slope depositional systems: component facies, stratigraphic architecture, and classification. AAPG Bull. 82, 569–595. https://doi.org/10.1306/1D9BC5BB-172D-11D7-8645000102C1865D.
Gardner, J.V., Mayer, L.A., Clarke, J.E.H., 2000. Morphology and processes in lake Tahoe (California-Nevada). GSA Bull 112, 736–746. https://doi.org/10.1130/0016-7606(2000)112<736:MAPILT>2.0.CO;2.
Gawthorpe, R.L., Leeder, M.R., 2000. Tectono-sedimentary evolution of active extensional basins. Basin Res. 12, 195–218. https://doi.org/10.1111/j.1365-2117.2000.00121.x.
Gee, M.J.R., Masson, D.G., Watts, A.B., Allen, P.A., 1999. The Saharan debris flow: an insight into the mechanics of long runout submarine debris flows. Sedimentology 46, 317–335. https://doi.org/10.1046/j.1365-3091.1999.00215.x.
Gong, C.L., Steel, R.J., Wang, Y.M., Lin, C.S., Olariu, C., 2016. Shelf-margin architecture variability and its role in sediment-budget partitioning into deep-water areas. Earth Sci. Rev. 154, 72–101. https://doi.org/10.1016/j.earscirev.2015.12.003.
Hackbarth, C.J., Shaw, R.D., 1994. Morphology and stratigraphy of a mid-Pleistocene turbidite leveed channel from seismic, core and log data, northeastern Gulf of Mexico. In: Weimer, P., Bouma, A.H., Perkins, B.F. (Eds.), Submarine Fans and Turbidite Systems: Gulf Coast Society of the Society of Economic Paleontologists and Mineralogists Foundation, 15th Annual Research Conference, pp. 127–133. https://doi.org/10.5724/gcs.94.15.0137.
Hampton, M.A., 1972. The role of subaqueous debris flow in generating turbidity currents. J. Sediment. Res. 42, 775–793. https://doi.org/10.1306/74D7262B-2B21-11D7-8648000102C1865D.
Hampton, M.A., 1975. Competence of fine-grained debris flows. J. Sediment. Res. 45, 834–844. https://doi.org/10.1306/212F6E5B-2B24-11D7-8648000102C1865D.
Hampton, M.A., Lee, H.J., Locat, J., 1996. Submarine landslides. Rev. Geophys. 34, 33–59. https://doi.org/10.1029/95RG03287.
Haughton, P.D., Barker, S.P., McCaffrey, W.D., 2003. 'Linked' debrites in sand-rich turbidite systems-origin and significance. Sedimentology 50, 459–482. https://doi.org/10.1046/j.1365-3091.2003.00560.x.
Haughton, P., Davis, C., McCaffrey, W., Barker, S., 2009. Hybrid sediment gravity flow deposits-classification, origin and significance. Mar. Petrol. Geol. 26, 1900–1918. https://doi.org/10.1016/j.marpetgeo.2009.02.012.
Heezen, B.C., Ewing, M., 1952. Turbidity currents and submarine slumps, and the 1929 Grand Banks earthquake. Am. J. Sci. 250, 849–873. https://doi.org/10.2475/ajs.250.12.849.
Hiscott, R.N., James, N.P., 1985. Carbonate debris flows, Cow Head Group, western Newfoundland. J. Sediment. Res. 55, 735–745. https://doi.org/10.1306/212F87D3-2B24-11D7-8648000102C1865D.
Hu, S.B., O'Sullivan, P.B., Raza, A., Kohn, B.P., 2001. Thermal history and tectonic subsidence of the Bohai Basin, northern China: a Cenozoic rifted and local pull-apart basin. Phys. Earth Planet. In. 126, 221–235. https://doi.org/10.1016/S0031-9201(01)00257-6.
Ito, M., 2008. Downfan transformation from turbidity currents to debris flows at a channel-to-lobe transitional zone: the lower Pleistocene Otadai Formation, Boso Peninsula, Japan. J. Sediment. Res. 78, 668–682. https://doi.org/10.2110/jsr.2008.076.
Iverson, R.M., 1997. The physics of debris flows. Rev. Geophys. 35, 245–296. https://doi.org/10.1029/97RG00426.
Jin, Q., Wang, R., Zhu, G.Y., Zheng, Y., Rong, Q.H., 2005. The lacustrine Liangjialou Fan in the Dongying Rift, eastern China: deep-water reservoir sandstones in a nonmarine rift basin. J. Petrol. Geol. 28, 397–411. https://doi.org/10.1111/j.1747-5457.2005.tb00090.x.
Johnson, A.M., 1970. Physical Processes in Geology: A Method for Interpretation of Natural Phenomena; Intrusions in Igneous Rocks, Fractures, and Folds. Flow of Debris and Ice. Freeman, Cooper, San Francisco, p. 577.
Johnson, A.M., 1984. Debris flow. In: Brunsden, D., Prior, D.B. (Eds.), Slope Instability. Wiley, Chichester, pp. 257–361.
Kane, I.A., Pontén, A.S., 2012. Submarine transitional flow deposits in the Paleogene Gulf of Mexico. Geology 40, 1119–1122. https://doi.org/10.1130/G33410.1.
Kane, I.A., Pontén, A.S., Vangdal, B., Eggenhuisen, J.T., Hodgson, D.M., Spychala, Y.T., 2017. The stratigraphic record and processes of turbidity current transformation across deep-marine lobes. Sedimentology 64, 1236–1273. https://doi.org/10.1111/sed.12346.
Kim, S.B., Chough, S.K., Chun, S.S., 1995. Bouldery deposits in the lowermost part of the Cretaceous Kyokpori Formation, SW Korea: cohesionless debris flows and debris falls on a steep-gradient delta slope. Sediment. Geol. 98, 97–119. https://doi.org/10.1016/0037-0738(95)00029-8.
Koo, W.M., Olariu, C., Steel, R.J., Olariu, M.I., Carvajal, C.R., Kim, W., 2016. Coupling between shelf-edge architecture and submarine-fan growth style in a supply-dominated margin. J. Sediment. Res. 86, 613–628. https://doi.org/10.2110/jsr.2016.42.
Kremer, K., Corella, J.P., Adatte, T., Garnier, E., Zenhäusern, G., Girardclos, S., 2015. Origin of turbidites in deep Lake Geneva (France-Switzerland) in the last 1500 years. J. Sediment. Res. 85, 1455–1465. https://doi.org/10.2110/jsr.2015.92.
Laberg, J.S., Vorren, T.O., 1995. Late Weichselian submarine debris flow deposits on the Bear Island Trough mouth fan. Mar. Geol. 127, 45–72. https://doi.org/10.1016/0025-3227(95)00055-4.
Lawton, T.F., 2019. Laramide sedimentary basins and sediment-dispersal systems. In: The sedimentary basins of the United States and Canada. Elsevier,

pp. 529–557. https://doi.org/10.1016/B978-0-444-63895-3.00013-9.
Lee, S.H., Chough, S.K., Back, G.G., Kim, Y.B., Sung, B.S., 1999. Gradual downslope change in high-resolution acoustic characters and geometry of large-scale submarine debris lobes in Ulleung Basin, East Sea (Sea of Japan), Korea. Geo Mar. Lett. 19, 254–261. https://doi.org/10.1007/s003670050116.
Li, J., 1983. The main features of the mudflow in Jiang-Jia Ravine. Zeitsch Geomorphol 27, 325–341. https://doi.org/10.1127/zfg/27/1983/325.
Li, C.Y., 2005. Study on the Forming Mechanism of the Slumped Turbidite and the Controlling Sandbody Model of High Freqency Base-Level Cycle of Dongying Deltas. China University of Geoscience, Beijing), Beijing. Ph.D. Dissertation.
Li, S.J., Zheng, D.S., Jiang, Z.X., Hu, B., Wang, J.X., Jiao, Y.H., 2005. Water depth of palaeo-lacustrine basin recovered by dominance diversity of Ostracoda: an example from sedimentary period of the Member 3 of Shahejie Formation of Paleogene in Dongying sag, Shandong Province. J Palaeogeog 7, 399–404 (in Chinese).
Li, X.B., Yang, Z.L., Wang, J., Liu, H.Q., Chen, Q.L., Rong, W.Y., Liao, J.B., Li, Z.Y., 2016. Mud-coated intraclasts: a criterion for recognizing sandy mass-transport deposits-deep-lacustrine massive sandstone of the Upper Triassic Yanchang Formation, Ordos Basin, Central China. J. Asian Earth Sci. 129, 98–116. https://doi.org/10.1016/j.jseaes.2016.06.007.
Lin, C.S., Pan, Y.L., Xiao, J.X., Kong, F.X., Liu, J.Y., Zheng, H.R., 2000. Structural slope-break zone: Key concept for stratigraphic sequence analysis and petroleum forecasting in fault subsidence basins. Earth Sci. J. China Univ. Geosci. 25, 260–266 (in Chinese).
Liu, J.P., Xian, B.Z., Wang, J.H., Ji, Y.L., Lu, Z.Y., Liu, S.J., 2017. Sedimentary architecture of a sub-lacustrine debris fan: Eocene Dongying Rift, Bohai Bay Basin, east China. Sediment. Geol. 362, 66–82. https://doi.org/10.1016/j.sedgeo.2017.09.014.
Liu, J.T., Hsu, R.T., Hung, J.J., Chang, Y.P., Wang, Y.H., Rendle-Bühring, R.H., Lee, C.L., Huh, C.A., Yang, R.J., 2021. From the highest to the deepest, The Gaoping River–Gaoping Submarine Canyon dispersal system. Earth Sci. Rev. 153, 274–300. https://doi.org/10.1016/j.earscirev.2015.10.012.
Liu, J.P., Xian, B.Z., Tan, X.F., Zhang, L., Su, M., Wu, Q.R., Wang, Z., Chen, P., He, Y.X., Zhang, S.H., Li, J., Gao, Y., Yu, Q.H., 2022. Depositional process and dispersal pattern of a faulted margin hyperpycnal system: The Eocene Dongying Depression, Bohai Bay Basin, China. Mar. Petrol. Geol. 135, 105405. https://doi.org/10.1016/j.marpetgeo.2021.105405.
Lowe, D.R., 1976. Subaqueous liquefied and fluidized sediment flow and their deposits. Sedimentology 23, 285–308. https://doi.org/10.1111/j.1365-3091.1976.tb00051.x.
Lowe, D.R., 1979. Sediment gravity flows: their classifications and some problems of application to natural flows and deposits. In: Doyle, L.J., Pilkey, O.H. (Eds.), Geology of Continental Slopes, vol. 27. SEPM Special Publication, pp. 75–82. https://doi.org/10.2110/pec.79.27.0075.
Lowe, D.R., 1982. Sediment gravity flows: II depositional models with special reference to the deposits of high-density turbidity currents. J. Sediment. Res. 52, 279–297. https://doi.org/10.1306/212F7F31-2B24-11D7-8648000102C1865D.
Maar, J.D.G., 1999. Experiments on Subaqueous Sandy Gravity Flows: Flow Dynamics and Deposit Structures. MSc. University of Minnesota, Thesis.
Marr, J.G., Harff, P.A., Shanmugam, G., Parker, G., 2001. Experiments on subaqueous sandy gravity flows: the role of clay and water content in flow dynamics and depositional structures. GSA Bull 113, 1377–1386. https://doi.org/10.1130/0016-7606(2001)113<1377:EOSSGF>2.0.CO;2.
Masson, D.G., Harbitz, C.B., Wynn, R.B., Pedersen, G., Løvholt, F., 2006. Submarine landslides: processes, triggers and hazard prediction. Phil. Trans. Roy. Soc. Lond.: Math. Phys. Eng. Sci. 364, 2009–2039. https://doi.org/10.1098/rsta.2006.1810.
Middleton, G.V., Hampton, M.A., 1973. Sediment gravity flows: mechanics of flow and deposition. In: Middleton, G.V., Bouma, A.H. (Eds.), Co-Chairmen), Turbidites and Deep Water Sedimentation. SEPM Pacific Section, Short Course, pp. 1–38.
Middleton, G.V., Hampton, M.A., 1976. Subaqueous sediment transport and deposition by sediment gravity flows. In: Stanley, D.J., Swift, D.J.P. (Eds.), Marine Sediment Transport and Environmental Management. Wiley, New York, pp. 197–218.
Migeon, S., Ducassou, E., Le Gonidec, Y., Rouillard, P., Mascle, J., Revel-Rolland, M., 2010. Lobe construction and sand/mud segregation by turbidity currents and debris flows on the western Nile deep-sea fan (Eastern Mediterranean). Sediment. Geol. 229, 124–143. https://doi.org/10.1016/j.sedgeo.2010.02.011.
Mohrig, D., Ellis, C., Parker, G., Whipple, K.X., Hondzo, M., 1998. Hydroplaning of subaqueous debris flows. GSA Bull 110, 387–394. https://doi.org/10.1130/0016-7606(1998)110<0387:HOSDF>2.3.CO;2.
Morton, D.M., Campbell, R.H., 1974. Spring mudflows at Wrightwood, southern California. Q J Eng Geol Hydroge 7, 377–384. https://doi.org/10.1144/GSL.QJEG.1974.007.04.
Mulder, T., Alexander, J., 2001. The physical character of subaqueous sedimentary density flows and their deposits. Sedimentology 48, 269–299. https://doi.org/10.1046/j.1365-3091.2001.00360.x.
Muravchik, M., Henstra, G.A., Eliassen, G.T., Gawthorpe, R.L., Leeder, M., Kranis, H., Skourtsos, E., Andrews, J., 2020. Deep-water sediment transport patterns and basin floor topography in early rift basins: Plio-Pleistocene syn-rift of the Corinth Rift, Greece. Basin Res. 32, 1184–1212. https://doi.org/10.1111/bre.12423.
Mutti, E., Normark, W.R., 1991. An integrated approach to the study of turbidite systems. In: Seismic Facies and Sedimentary Processes of Submarine Fans and Turbidite Systems. Springer, New York, NY, pp. 75–106. https://doi.org/10.1007/978-1-4684-8276-8_4.
Mutti, E., Bernoulli, D., Ricci Lucchi, F., Tinterri, R., 2009. Turbidites and turbidity currents from Alpine "Flysch" to the exploration of continental margins. In: McKenzie, J.A., Bernoulli, D., Cita, M.B. (Eds.), Symposium on Major Discoveries in Sediment Geol in the Mediterranean Realm from a Historical Perspective to New Development. Sedimentology, vol. 56, pp. 267–318. https://doi.org/10.1111/j.1365-3091.2008.01019.x.
Nemec, W., 1990. Aspects of sediment movement on steep delta slopes. In: Colella, A., Prior, D.B. (Eds.), Coarse-Grained Deltas, vol. 10. IAS Special Publication, pp. 29–73. https://doi.org/10.1002/9781444303858.ch3.
Nisbet, E.G., Piper, D.J.W., 1998. Giant submarine landslides: slumps, mega turbidites and their impart. Nature 392, 329–330. https://doi.org/10.1038/32765.
Normark, W.R., 1970. Growth patterns of deep sea fans. AAPG Bull. 54, 2170–2195. https://doi.org/10.1306/5D25CC79-16C1-11D7-8645000102C1865D.
O'Brien, J.S., Julien, P.Y., 1988. Laboratory analysis of mudflow properties. J. Hydraul. Eng. 114, 877–887. https://doi.org/10.1061/(ASCE)0733-9429.
Parsons, J.D., Whipple, K.X., Simoni, A., 2001. Experimental study of the grain-flow, fluid mud transition in debris flows. J. Geol. 109, 427–447. https://doi.org/10.1086/320798.
Peng, J.W., 2021. Sedimentology of the Upper Pennsylvanian organic-rich Cline Shale, Midland Basin: From gravity flows to pelagic suspension fallout. Sedimentology 68, 805–833. https://doi.org/10.1111/sed.12811.
Peng, J.W., Hu, Z.Q., Feng, D.J., Wang, Q.R., 2022. Sedimentology and sequence stratigraphy of lacustrine deep-water fine-grained sedimentary rocks: The Lower Jurassic Dongyuemiao Formation in the Sichuan Basin, Western China. Mar. Petrol. Geol. 146, 105933. https://doi.org/10.1016/j.marpetgeo.2022.105933.
Piper, D.J.W., Aksu, A.E., 1987. The source and origin of the 1929 Grand Banks turbidity current inferred from sediment budgets. Geo Mar. Lett. 7, 177–182. https://doi.org/10.1007/BF02242769.
Piper, D.J.W., Cochonat, P., Morrison, M.L., 1999. The sequence of events around the epicentre of the 1929 Grand Banks earthquake: initiation of debris flows and turbidity current inferred from sidescan sonar. Sedimentology 46, 79–97. https://doi.org/10.1046/j.1365-3091.1999.00204.x.
Plink-Björklund, P., Steel, R.J., 2004. Initiation of turbidity currents: outcrop evidence for Eocene hyperpycnal flow turbidites. Sediment. Geol. 165, 29–52. https://doi.org/10.1016/j.sedgeo.2003.10.013.
Plint, A.G., 1986. Slump blocks, intraformational conglomerates and associated erosional structures in Pennsylvanian fluvial strata of eastern Canada. Sedimentology 33, 387–399. https://doi.org/10.1111/j.1365-3091.1986.tb00543.x.
Posamentier, H.W., Kolla, V., 2003. Seismic geomorphology and stratigraphy of depositional elements in deep-water settings. J. Sediment. Res. 73, 367–388. https://doi.org/10.1306/111302730367.
Postma, G., Nemec, W., Kleinspehn, K.L., 1988. Large floating clasts in turbidites: a mechanism for their emplacement. Sediment. Geol. 58, 47–61. https://doi.org/10.1016/0037-0738(88)90005-X.
Prélat, A., Hodgson, D.M., Flint, S.S., 2009. Evolution, architecture and hierarchy of distributary deep-water deposits: a high-resolution outcrop investigation from the Permian Karoo Basin, South Africa. Sedimentology 56, 2132–2154. https://doi.org/10.1111/j.1365-3091.2009.01073.x.
Prélat, A., Covault, J.A., Hodgson, D.M., Fildani, A., Flint, S.S., 2010. Intrinsic controls on thenrange of volumes, morphologies, and dimensions of submarine lobes. Sediment. Geol. 232, 66–76. https://doi.org/10.1016/j.sedgeo.2010.09.010.
Qiu, G.Q., Wang, J.F., Zhang, X., Li, C.X., 2001. Preliminary study on stratigraphy architecture of middle-Shasan Dongying delta and its significance to hydrocarbon exploration. J. Tongji Univ. 29, 1195–1199. https://doi.org/10.3969/j.issn.1000-0550.2001.04.015 (in Chinese).
Reading, H.G., Richards, M., 1994. Turbidite systems in deep-water basin margins classified by grain size and feeder system. AAPG Bull. 78, 792–822. https://doi.org/10.1306/A25FE3BF-171B-11D7-8645000102C1865D.
Sanders, J.E., 1965. Primary sedimentary structures formed by turbidity currents and related resedimentation mechanisms. In: Middleton, G.V. (Ed.), Primary Sedimentary Structures and Their Hydrodynamic Interpretation, vol. 12. SEPM Special Publication, pp. 192–219. https://doi.org/10.2110/pec.65.08.0192.
Sawyer, D.E., Flemings, P.B., Buttles, J., Mohrig, D., 2012. Mudflow transport behavior and deposit morphology: Role of shear stress to yield strength ratio in subaqueous experiments. Mar. Geol. 307, 28–39. https://doi.org/10.1016/j.margeo.2012.01.009.
Shanmugam, G., 1996. High-density turbidity currents: are they sandy debris flows? J. Sediment. Res. 66, 2–10. https://doi.org/10.1306/D426828E-2B26-11D7-8648000102C1865D.
Shanmugam, G., 2000. 50 years of the turbidite paradigm (1950s-1990s): deep-water processes and facies models—a critical perspective. Mar. Petrol. Geol. 17, 285–342. https://doi.org/10.1016/S0264-8172(99)00011-2.
Shanmugam, G., 2012. New perspectives on deep-water sandstones: origin, recognition, initiation, and reservoir quality. In: Handbook of Petroleum Exploration and Production, vol. 9. Elsevier, Amsterdam, p. 524.
Shanmugam, G., 2013. New perspectives on deep-water sandstones: Implications. Petrol. Explor. Dev. 40, 316–324. https://doi.org/10.1016/S1876-3804(13)60038-5.
Shanmugam, G., 2016. Submarine fans: a critical retrospective (1950-2015). J Palaeogeog 5, 110–184. https://doi.org/10.1016/j.jop.2015.08.011.
Shanmugam, G., Moiola, R.J., 1994. An unconventional model for the deep-water sandstones of the Jackfork Group (Pennsylvanian), Ouachita Mountains,

Arkansas and Oklahoma. In: Submarine Fans and Turbidite Systems: Gulf Coast Section of SEPM 15th Annual Research Conference, pp. 311–326. https://doi.org/10.5724/gcs.94.15.0335.
Shanmugam, G., Lehtonen, L.R., Straume, T., Syvertsen, S.E., Hodgkinson, R.J., Skibeli, M., 1994. Slump and debris-flow dominated upper slope facies in the Cretaceous of the Norwegian and northern North Seas (61-67 N): Implications for sand distribution. AAPG Bull. 78, 910–937. https://doi.org/10.1306/A25FE3E7-171B-11D7-8645000102C1865D.
Shanmugam, G., Bloch, R.B., Mitchell, S.M., Beamish, G.W., Hodgkinson, R.J., Damuth, J.E., Straume, T., Syvertsen, S.E., Shields, K.E., 1995. Basin-floor fans in the North Sea: sequence stratigraphic models vs. sedimentary facies. AAPG Bull. 79, 477–511. https://doi.org/10.1306/8D2B1570-171E-11D7-8645000102C1865D.
Sharp, R.P., Nobles, L.H., 1953. Mudflow of 1941 at Wrightwood, Southern California. GSA Bull 64, 547–560. https://doi.org/10.1130/0016-7606(1953)64[547:MOAWSC]2.0.CO;2.
Shepard, F.P., 1932. Landslide modifications of submarine valleys. Eos, Transactions American Geophysical Union 13, 226–230. https://doi.org/10.1029/TR013i001p00226.
Soh, W., 1989. Coarse clast dominant submarine debrite, the Mio-Pliocene Fujikawa Group, central Japan. In: Taira, A., Mazuda, F. (Eds.), Sedimentary Facies in the Active Plate Margin. Terra Scientific Publishing, Tokyo, pp. 495–510.
Sohn, Y.K., 2000. Depositional processes of submarine debris flows in the Miocene fan deltas, Pohang Basin, SE Korea with special reference to flow transformation. J. Sediment. Res. 70, 491–503. https://doi.org/10.1306/2DC40922-0E47-11D7-8643000102C1865D.
Sohn, Y.K., Rhee, C.W., Kim, B.C., 1999. Debris flow and hyperconcentrated flood-flow deposits in an alluvial fan, northwestern part of the Cretaceous Yongdong Basin, Central Korea. J. Geol. 107, 111–132. https://doi.org/10.1086/314334.
Sømme, T.O., Helland-Hansen, W., Granjeon, D., 2009. Impact of eustatic amplitude variations on shelf morphology, sediment dispersal, and sequence stratigraphic interpretation: Icehouse versus greenhouse systems. Geology 37, 587–590. https://doi.org/10.1130/G25511A.1.
Southern, S.J., Kane, I.A., Warchoł, M.J., Porten, K.W., McCaffrey, W.D., 2017. Hybrid event beds dominated by transitional-flow facies: character, distribution and significance in the Maastrichtian Springar Formation, north-west Vøring Basin, Norwegian Sea. Sedimentology 64, 747–776. https://doi.org/10.1111/sed.12323.
Soutter, E.L., Kane, I.A., Huuse, M., 2018. Giant submarine landslide triggered by Paleocene mantle plume activity in the North Atlantic. Geology 46, 511–514. https://doi.org/10.1130/G40308.1.
Steel, R.J., Olsen, T., Armentrout, J.M., Rosen, N.C., 2002. Clinoforms, clinoform trajectories and deepwater sands. In: Sequence-stratigraphic Models for Exploration and Production: Evolving Methodology, Emerging Models and Application Histories: Gulf Coast Section SEPM 22nd Research Conference, Houston, Texas, pp. 367–381. https://doi.org/10.5724/gcs.02.22.0367.
Stow, D.A., Johansson, M., 2000. Deep-water massive sands: nature, origin and hydrocarbon implications. Mar. Petrol. Geol. 17, 145–174. https://doi.org/10.1016/S0264-8172(99)00051-3.
Stow, D.A., Mayall, M., 2000. Deep-water sedimentary systems: new models for the 21st century. Mar. Petrol. Geol. 17, 125–135. https://doi.org/10.1016/S0264-8172(99)00064-1.
Talling, P.J., 2014. On the triggers, resulting flow types and frequencies of subaqueous sediment density flows in different settings. Mar. Geol. 352, 155–182. https://doi.org/10.1016/j.margeo.2014.02.006.
Talling, P.J., Amy, L.A., Wynn, R.B., Peakall, J., Robinson, M., 2004. Beds comprising debrite sandwiched within co-genetic turbidite: origin and widespread occurrence in distal depositional environments. Sedimentology 51, 163–194. https://doi.org/10.1111/j.1365-3091.2004.00617.x.
Talling, P.J., Wynn, R.B., Masson, D.G., Frenz, M., Cronin, B.T., Schiebel, R., Akhmetzhanov, A.M., Dallmeier-Tiessen, S., Benetti, S., Weaver, P.P.E., Georgiopoulou, A., Zuhlsdorff, C., Amy, L.A., 2007. Onset of submarine debris flow deposition far from original giant landslide. Nature 450, 541–544. https://doi.org/10.1038/nature06313.
Talling, P.J., Malgesini, G., Sumner, E.J., Amy, L.A., Felletti, F., Blackbourn, G., Nutt, C., Wilcox, C., Harding, I.C., Akbari, S., 2012. Planform geometry, stacking pattern, and extrabasinal origin of low strength and intermediate strength cohesive debris flow deposits in the Marnoso-arenacea Formation, Italy. Geosphere 8, 1207–1230. https://doi.org/10.1130/GES00734.1.
Tan, M., Sun, H., Fu, Y., Zhang, X., Cui, H., Ma, H., 2022. Hybrid event bed characteristics and its role in high-frequency facies change of the Upper Triassic submarine fan in the West Qinling area of NE Tibetan Plateau. Mar. Petrol. Geol. 146, 105937. https://doi.org/10.1016/j.marpetgeo.2022.105937.
Tian, Z.Q., 2004. The Fine Description of Ying 11 Es3 Low Permeability Reservoir, the Numerical Simulation and Analysis of Horizontal Well-Development in Dongxin Oil Field. Graduate School of Chinese Academy of Sciences (Guangzhou Institute of Geochemistry), PhD dissertation, pp. 1–150 (in Chinese).
Tian, R.H., Xian, B.Z., Wu, Q.R., Shu, Q.L., Liu, J.P., Zhang, W.M., Wang, Z., Li, Q., Rahman, N., Gao, Y.K., Wang, J.W., 2023. Turbidite system controlled by fault interaction and linkage on a slope belt of rift basin: Zhanhua depression, Bohai Bay Basin, China. Mar. Petrol. Geol. 155, 106377. https://doi.org/10.1016/j.marpetgeo.2023.106377.
Walker, R.G., 1978. Deep-water sandstone facies and ancient submarine fans: models for exploration for stratigraphic traps. AAPG Bull. 62, 932–966. https://doi.org/10.1306/C1EA4F77-16C9-11D7-8645000102C1865D.
Walsh, J.P., Corbett, R., Mallinson, D., Goni, M., Dail, M., Loewy, C., Marciniak, K., Ryan, K., Smith, C., Stevens, A., Summers, B., Tesi, T., 2006. Mississippi delta mudflow activity and 2005 Gulf hurricanes. Eos, Transactions American Geophysical Union 87, 477–478. https://doi.org/10.1029/2006EO440002.
Wang, X., Wang, Y., Tan, M., Cai, F., 2020. Deep-water deposition in response to sea-level fluctuations in the past 30 kyr on the northern margin of the South China Sea. Deep Sea Res Pt I 163, 103317. https://doi.org/10.1016/j.dsr.2020.103317.
Weimer, P., Pettingill, H.S., 2007. Deep-water exploration and production: A global overview. Atlas of deep-water outcrops. In: AAPG Studies in Geology, vol. 56. https://doi.org/10.1306/12401007St56285.
Weirich, F.H., 1988. Field evidence for hydraulic jumps in subaqueous sediment gravity flows. Nature 332, 626–629. https://doi.org/10.1038/332626a0.
Whipple, K.X., Dunne, T., 1992. The influence of debris-flow rheology on fan morphology. Owens Valley, California. GSA Bull 104, 887–900. https://doi.org/10.1130/0016-7606(1992)104<0887:TIODFR>2.3.CO;2.
Woodcock, N.H., 1976. Structural style in slump sheets: Ludlow series, Powys, Wales. J Geol Soc London 132, 399–415. https://doi.org/10.1144/gsjgs.132.4.039.
Wu, Q.R., Xian, B.Z., Gao, X.Z., Bai, Q.L., Wang, Z., Liu, J.P., Chen, P., Li, Y.Z., Rahman, N., Tian, R.H., Zhang, W.M., Zhang, H.Z., 2022. Differences of sedimentary triggers and depositional architecture of lacustrine turbidites from normal regression to forced regression: Eocene Dongying depression, Bohai Bay Basin, East China. Sediment. Geol. 439, 106222. https://doi.org/10.1016/j.sedgeo.2022.106222.
Xian, B.Z., An, S.Q., Shi, W.H., 2014. Subaqueous debris flow: hotspots and advances of deep-water sedimention. Geol. Rev. 60, 39–51. https://doi.org/10.3969/j.issn.0371-5736.2014.01.004 (in Chinese).
Xian, B.Z., Liu, J.P., Dong, Y.L., Lu, Z.Y., He, Y.X., Wang, J.H., 2017. Classification and facies sequence model of subaqueous debris flows. Acta Geol Sin-Engl (English Edition) 91, 751–752. https://doi.org/10.1111/1755-6724.13140.
Xian, B.Z., Wang, J.H., Liu, J.P., Dong, Y.L., Gong, C.L., Lu, Z.Y., 2018. Delta-fed turbidites in a lacustrine rift basin: the Eocene Dongying Rift, Bohai Bay Basin, East China. Aust. J. Earth Sci. 65, 135–151. https://doi.org/10.1080/08120099.2018.1401558.
Yang, R.C., Jin, Z.J., Van Loon, A.J., Han, Z.Z., Fan, A.P., 2017. Climatic and tectonic controls of lacustrine hyperpycnite origination in the Late Triassic Ordos Basin, central China, Implications for unconventional petroleum development. AAPG Bull. 101, 95–117. https://doi.org/10.1306/06101615095.
Yang, T., Cao, Y.C., Liu, K.Y., Tian, J.C., Zavala, C., Wang, Y.Z., 2020. Gravity-flow deposits caused by different initiation processes in a deep-lake system. AAPG Bull. 104, 1463–1499. https://doi.org/10.1306/03172017081.
Yang, T., Cao, Y.C., Liu, H.N., 2023. Highstand sublacustrine fans: The role of a sudden increase in sediment supply. Basin Res. 1–23. https://doi.org/10.1111/bre.12762.
Zavala, C., Arcuri, M., 2016. Intrabasinal and extrabasinal turbidites: Origin and distinctive characteristics. Sediment. Geol. 337, 36–54. https://doi.org/10.1016/j.sedgeo.2016.03.008.
Zhang, J.G., Jiang, Z.X., Liang, C., Wu, J., Xian, B.Z., Li, Q., 2016. Lacustrine massive mudrock in the Eocene Jiyang Depression, Bohai Bay Basin, China: Nature, origin and significance. Mar. Petrol. Geol. 77, 1042–1055. https://doi.org/10.1016/j.marpetgeo.2016.08.008.
Zou, C.N., Wang, L., Li, Y., Tao, S.Z., Hou, L.H., 2012. Deep-lacustrine transformation of sandy debrites into turbidites, Upper Triassic, Central China. Sediment. Geol. 265, 143–155. https://doi.org/10.1016/j.sedgeo.2012.04.004.